

UNCERTAINTY ANALYSIS OF COMBUSTION AND SPECTROSCOPY
MEASUREMENTS

by

ALEXANDER JOEL-ERIK LARSSON

(Under the Direction of Brandon Rotavera)

ABSTRACT

The present work focuses on the development and application of methodologies for (i) temperature profile characterization within a jet-stirred reactor (JSR) for quantification of uncertainty in concentration profiles measured in combustion experiments, and (ii) calculating uncertainty in species concentration used in absorption spectroscopy experiments. Temperature profiles were measured at atmospheric pressure, using a 1.6-mm-diameter K-type thermocouple positioned inside of the 30-cm³ JSR as a function of residence time, reactor temperature, and pre-heater temperature. For the spectroscopy measurements, uncertainty analysis focused on gas-phase concentrations used to determine absorption cross-sections. The JSR analysis consisted of measuring temperature profiles, $T(x)$, for residence times of 500 ms, 1000 ms, and 2000 ms, and reactor temperatures of 500 K, 750 K, and 1200 K at 20 positions within the reactor. The measurements led to quantified thermal gradients, dT/dx , which were utilized to determine the dependence of dT/dx on volumetric flow rate and temperature.

INDEX WORDS: Uncertainty analysis, errors, chemical kinetics, statistics.

UNCERTAINTY ANALYSIS OF COMBUSTION AND SPECTROSCOPY
MEASUREMENTS

by

ALEXANDER JOEL-ERIK LARSSON

B.S., University of Georgia, 2018

A Thesis Submitted to the Graduate Faculty of The University of Georgia in Partial
Fulfillment of the Requirements for the Degree

MASTER OF SCIENCE

ATHENS, GEORGIA

2020

© 2020

Alexander Joel-Erik Larsson

All Rights Reserved

UNCERTAINTY ANALYSIS OF COMBUSTION AND SPECTROSCOPY
MEASUREMENTS

by

ALEXANDER JOEL-ERIK LARSSON

Major Professor: Brandon Rotavera

Committee: Rawad Saleh
Ben Davis

Electronic Version Approved:

Ron Walcott
Interim Dean of the Graduate School
The University of Georgia
May 2020

DEDICATION

I am dedicating this thesis to my loving family, Kent, Rebecca, and Annika Larsson, for always supporting me and helping me see my dreams come true. I know it has not been easy, but it means the world to know you will always stand in my corner, no matter the challenge. You have instilled traditional values, a love for learning, and a strong work ethic that has allowed me to reach this milestone. You have taught me that anything can be achieved if you put your mind to it, and this thesis is living proof to that. Combining athletics and academics was never easy, and especially difficult while in graduate school.

ACKNOWLEDGEMENTS

First, I would like to thank Dr. Brandon Rotavera for accepting me to be a part of his research team, in spite of not having any research background. I would also like to thank him for his continuous support during my two years as a part of the Rotavera Group at the University of Georgia, lifting me up when I needed help, and providing motivation when going through tough times. He has shown me what it is to be a professional engineer, and I hope I can emulate that in my own future career.

Second, I would also like to thank my fellow graduate students: Alanna Koritzke, Anna Donor, Josiah Breda-Nixon, Matthew Christianson, and graduate of the Rotavera Group, Jacob Davis. They have all helped me immensely and I would not be where I am today if it were not for their help in the laboratory. It is sad that we will part ways, but I will always be following you and wish you all good luck in your future endeavors.

Third, I would like to thank Mr. Hunt and his family for providing to the UGA College of Engineering with the Joel Terry Hunt Fellowship, of which I was the recipient 2018/2019 and 2019/2020. The scholarship truly relieved me of any financial burden while pursuing my Master's degree.

Lastly, I would like to thank the UGA Athletic Association for selecting me as the UGA recipient of the South Eastern Conference H. Boyd McWhorter Postgraduate Award. This award is very prestigious and I am truly honored to have been selected as the recipient. I would also like to thank the UGA Track and Field team for providing me with a full athletic scholarship to attend UGA 2013.

TABLE OF CONTENTS

	Page
ACKNOWLEDGEMENTS	v
LIST OF TABLES	viii
LIST OF FIGURES	ix
CHAPTER	
1 Introduction.....	1
Types of Uncertainty.....	2
Basics of Absorption Spectroscopy	4
Basics of Jet-Stirred Reactor (JSR) Experiments	5
Importance of Uncertainty Analysis	7
2 Background.....	11
3 Methodology for Uncertainty Quantification	14
Mass Flow Controller Uncertainty Analysis.....	14
Cross-Section Measurements Uncertainty Analysis.....	19
JSR Temperature Uncertainty Analysis.....	21
4 Uncertainty Measurements	27
Mass Flow Controllers.....	27
Cross-Section Measurements.....	30
JSR Temperature Measurements	31
5 Impact of Uncertainty on Cross-Sections and Species Profile	53

6 Conclusion and Future Work	56
REFERENCES	59

LIST OF TABLES

	Page
Table 1: Internal volumes for MFC experiment	16
Table 2: Sample test matrix for MFC uncertainty analysis	17
Table 3: Instruments used in cross-section uncertainty analysis	20
Table 4: Test matrix for the temperature gradient experiments.....	25
Table 5: Summarization of trends observed in the JSR temperature gradients	26
Table 6: Populated test matrix for JSR temperature gradient experiments	32
Table 7: Trend lines of Figure 20	34
Table 8: Trend lines of Figure 21	34
Table 9: Trend lines of Figure 22	35
Table 10: Trend lines of Figure 23	36
Table 11: Trend lines of Figure 24	37
Table 12: Trend lines of Figure 25	38
Table 13: Trend lines of Figure 26	39
Table 14: Trend lines of Figure 27	40
Table 15: Trend lines of Figure 28	40

LIST OF FIGURES

	Page
Figure 1: Definition of systematic error vs. random error	3
Figure 2: Differentiation between precision and accuracy	3
Figure 3: Schematic of VUV diagnostic	5
Figure 4: Schematic of a jet-stirred reactor.....	6
Figure 5: Image of the jet-stirred reactor	7
Figure 6: Application and example of the Arrhenius Equation	9
Figure 7: Graphical explanation of a temperature gradient	10
Figure 8: Experimental setup for MFC uncertainty analysis	15
Figure 9: Linear rotational thimble	22
Figure 10: Schematic of a jet-stirred reactor and thermocouple.....	22
Figure 11: Schematic of reactor setup	23
Figure 12: Schematic of reactor setup and location of the heaters	24
Figure 13: Time study of thermocouple equilibration	24
Figure 14: MFC analysis, 50 sccm O ₂	28
Figure 15: MFC analysis, 50 sccm N ₂	29
Figure 16: MFC analysis, 500 sccm O ₂	29
Figure 17: MFC analysis, 5000 sccm N ₂	30
Figure 18: Uncertainty calculator for chemical binary mixtures	31
Figure 19: Experimental results of JSR measurements	32

Figure 20: Temperature vs. location, $T_R=500$ K, $\tau=500$ ms	33
Figure 21: Temperature vs. location, $T_R=500$ K, $\tau=1000$ ms	34
Figure 22: Temperature vs. location, $T_R=500$ K, $\tau=2000$ ms	35
Figure 23: Temperature vs. location, $T_R=750$ K, $\tau=500$ ms	36
Figure 24: Temperature vs. location, $T_R=750$ K, $\tau=1000$ ms	37
Figure 25: Temperature vs. location, $T_R=750$ K, $\tau=2000$ ms	38
Figure 26: Temperature vs. location, $T_R=1200$ K, $\tau=500$ ms	39
Figure 27: Temperature vs. location, $T_R=1200$ K, $\tau=1000$ ms	39
Figure 28: Temperature vs. location, $T_R=1200$ K, $\tau=2000$ ms	40
Figure 29: Reaction volume inside the main heaters	43
Figure 30: Temperature vs. location, T_f-T_b , $T_R=500$ K, $\tau=500$ ms.....	44
Figure 31: Temperature vs. location, T_f-T_b , $T_R=500$ K, $\tau=1000$ ms.....	45
Figure 32: Temperature vs. location, T_f-T_b , $T_R=500$ K, $\tau=2000$ ms.....	45
Figure 33: Temperature vs. location, T_f-T_b , $T_R=750$ K, $\tau=500$ ms.....	46
Figure 34: Temperature vs. location, T_f-T_b , $T_R=750$ K, $\tau=1000$ ms.....	46
Figure 35: Temperature vs. location, T_f-T_b , $T_R=750$ K, $\tau=2000$ ms.....	47
Figure 36: Temperature vs. location, T_f-T_b , $T_R=1200$ K, $\tau=500$ ms.....	47
Figure 37: Temperature vs. location, T_f-T_b , $T_R=1200$ K, $\tau=1000$ ms.....	48
Figure 38: Temperature vs. location, T_f-T_b , $T_R=1200$ K, $\tau=2000$ ms.....	48
Figure 39: Preheater temperatures vs. voltage supplied by variacs	50
Figure 40: Main heater temperature vs. voltage supplied by variacs	50
Figure 41: Calculator for heating temperatures	51
Figure 42: Time study of heaters	52

Figure 43: VUV spectra with uncertainty bounds54

CHAPTER 1

INTRODUCTION

Speciation measurements from flow reactor experiments are critical to producing fundamental insight necessary for increasing the fidelity of computational chemical kinetics models used to design next-generation combustion systems. Of particular utility are concentration profiles for a given species measured as a function of temperature, pressure, and oxygen concentration. To provide boundaries to the accuracy of speciation measurements, uncertainty quantification is required for thermodynamic and flow conditions inside of a reactor. In addition, quantification of species requires prior measurements of absorption cross-sections, $\sigma(E)$, which are produced from spectroscopy experiments and depend on accurate determinations of concentration.

This thesis will focus on the uncertainties that are associated with the combustion and spectroscopy measurements in the Rotavera Group at the University of Georgia. According to the US Energy Outlook, fossil fuels will continue to be the leading source of energy for transportation for the next several of decades [1]. We study how biofuels combust under low-temperature and high-pressure conditions to see what byproducts are produced. This is important for several reasons, but primarily to study the feasibility to use biofuels as an additive to current gasoline and diesel mixtures, and its environmental impact. To accurately represent our data, a thorough analysis was required to account for any variation in the data. Uncertainties in laboratories generally originate in equipment. Electronic equipment uncertainty stems from the capability of storing binary data in bits,

and analog equipment uncertainty stems from the dial accuracy and mechanical fatigue from moving parts, such as a spring losing elasticity in a dynamometer. In the field of chemical kinetics, which is the study of how fast a certain reaction is, the effect of just 1% can be detrimental to the application of internal combustion engine design and its efficiency. This is of utmost importance for internal combustion applications within the transportation sector.

Types of Uncertainty

Measurement uncertainty encapsulates all errors that relate to how reliable an experimental parameter is. For this thesis, the term uncertainty will relate to measurements taken by laboratory equipment and their reliability in representing data. Uncertainty is a way of quantifying the magnitude of errors. Errors generally stem from two sources: systematic/bias, and random. Included in systematic bias is linearity and hysteresis. Systematic error is an offset from the true value and is addressed via instrument calibration. Random error is error that occurs with any measurement, and is expected to fall within the range of uncertainty for the instrument. Figure 1 includes a schematic of how scattering of measurements induces random errors, and illustrating the definition of systematic error as a line that is distanced from the true value. Random errors influence precision, and systematic errors influence the accuracy. Generally, for engineering applications, instruments have an uncertainty reported at 95% probability level (95% of the data will lie within two standard deviations, σ) [2]. Standard deviation is a measurement of variance, which is a measure of how far a measurement is from the mean. An important distinction must be made between precision and accuracy, as they are often mistaken to be interchangeable. Figure 2 illustrates the difference between

accuracy and precision. Figure 2a has high precision as the arrows are all in the same location, but are offset and give no indication to the accuracy of the measurement. Figure 2b introduces high precision and accuracy, as all arrows are in the same location and in the bulls-eye. Figure 2c indicates the case when accuracy as well as precision are both poor.

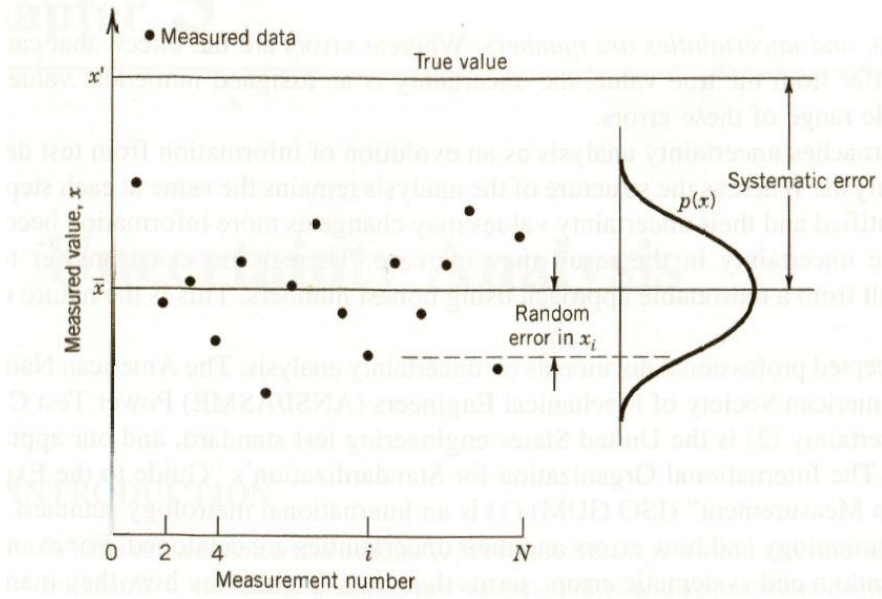


Figure 1: Systematic error vs. random error [2].

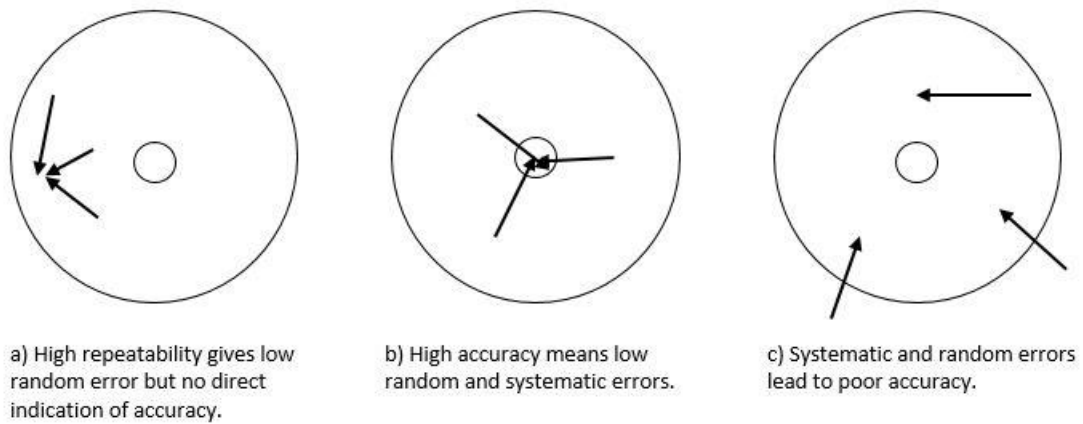


Figure 2: Illustration of random and systematic errors and accuracy, reproduced from [2].

A global uncertainty is the overall uncertainty for an experimental parameter. To calculate a global uncertainty, a common method used is known as the Root-Sum-Squares (RSS) method [2]. Equation 1 provides the general form of the RSS method, which may only be implemented when studying uncertainties in the same parameter, such as pressure. This is important because the units must be equal for the analysis to provide an accurate assumption on the propagation of errors. The errors analyzed in one set of experiments in the present work are in pressure, which are reported in Torr. The RSS method may be applied multiple times within an uncertainty analysis. The application of the RSS method is to collect all uncertainties stemming from the same parameter to achieve an overall assessment of the global uncertainty of a measurement.

$$u_x = \sqrt{\sum_{k=1}^K u_k^2} \quad (1)$$

Basics of Absorption Spectroscopy

In general, absorption spectroscopy is an analytical technique in chemistry to analyze the presence and quantity of a particular species. The technique utilized in the Rotavera group is *Vacuum Ultraviolet Spectroscopy* (VUV). The technique applies the Beer-Lambert Law, which is provided in Equation 2, where I_0 is the intensity of incident light, I is the intensity of absorbed light, σ is the absorption cross-section, c is the concentration of the species, and l is the optical path length. The parameter with a degree of freedom is the concentration, as it depends on the mixture that is being analyzed, and is inherently the dominating factor of uncertainty for the application of the equation. Later in Equation 6, a modified Beer-Lambert's Law is produced and is the one used in spectroscopy.

$$\log_{10} I_0/I = \sigma cl \quad (2)$$

An apparatus emits photons and excites the molecules, and a receiver analyzes how many photons passed through the vaporized chemical sample. A plot is generated of the absorption as a function of wavelength. Each chemical compound absorbs photoionization unique to the compound, which makes this spectrometric analysis very applicable for speciation experiments. VUV has a built-in library, and when samples are run through the spectrometer, the software will automatically compare the data with the library to find a match. Figure 3 includes a schematic of the procedure. A deuterium lamp excites the gas composition, which flows through a flow cell diluted with N₂ or He. The detector then detects how much of the light was absorbed by the species. Speciation experiments from ultraviolet spectroscopy are susceptible to uncertainties that must be accounted for. Concentration of the species is non-negligible due to chemical purity and any equipment that is operated, and thus the largest contributor to uncertainty in speciation experiments.

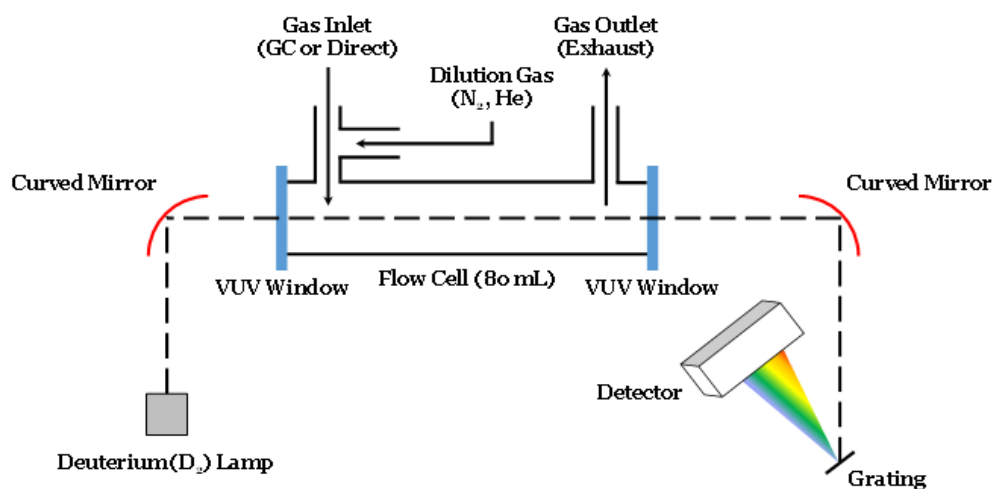


Figure 3: Schematic of the VUV diagnostic [3].

Basics of Jet-Stirred Reactor (JSR) Experiments

A jet-stirred reactor is a spherical flow reactor with tubular extensions that operates as a continuous flow apparatus and is used to study chemical kinetics [3]. A general schematic of a JSR is shown in Figure 4.

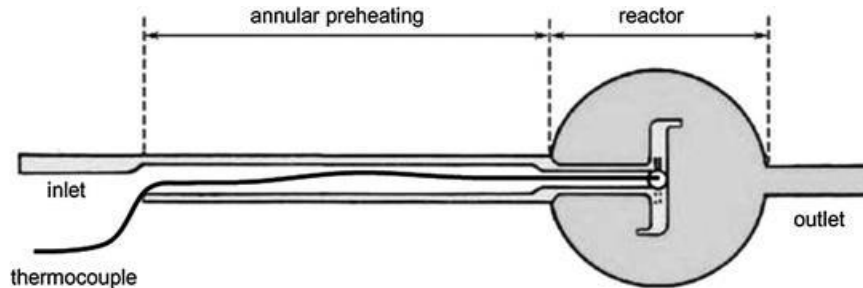


Figure 4: Schematic of a JSR. Gases and fuel enter through separate feeders and meet inside the reaction volume, and exit the jets that are centered in the reaction volume [3].

A chemical kinetic experiment in a JSR is conducted by flowing a sample of the desired hydrocarbon or biofuel, diluted with a diluent, such as N_2 , and combusted with oxygen in the reaction volume. This is achieved by the two separate gas flows flowing separately through a heating section where the gas is heated to the prescribed conditions. Both gas flows are then introduced to each other in the bulb section and then ejected through the jets. The sole purpose of the jets is to ensure the flow becomes turbulent to enhance the mixing and create a homogenous mixture. This mixture is then sampled downstream using a vacuum drawn sonic probe, which “freezes” the flow, which ensures no further reactions occur. This is important so the flow at the prescribed conditions is the flow that is analyzed. Figure 5 is an image of the JSR with an internal volume of 30 cm^3 and an internal diameter of approximately 3.8cm, with the four 1-mm diameter mixing jets in the center.



Figure 5: Image of the jet-stirred reactor. Direction of flow is downward.

Importance of Uncertainty Analysis

What is measured from the JSR experiments are the products that are formed from the chemical reaction of the fuel with oxygen, both qualitatively and quantitatively, using off-line diagnostics, which also have associated uncertainties. Chemical reactions break the fuel into intermediates throughout the reaction until the reaction is complete. Intermediates is a term for the products that generally are formed between the typical chemical reaction of a fuel and oxygen to carbon dioxide and water. However, for biofuel combustion and applications of Low Temperature Combustion (LTC) engines, the aim is to operate at low temperatures ($T < 1400$ K) and high pressures ($P > 20$ atm). There are knowledge gaps at these conditions, and present new challenges for the transportation sector. While operating at a lower temperature might entail lower fuel consumption, further analysis is needed to identify the intermediates that adversely affect air quality. In addition to the environmental aspect, different chemical kinetics will also adjust the ignition properties. Thus, it is imperative that analysis can be conducted on intermediates of biofuels.

As with any equipment, there are embedded uncertainties. To quantify data retrieved from the jet-stirred reactor with well-defined uncertainties, and because such data points are critical for their intended applications, it is highly imperative to conduct an uncertainty analysis. It should be noted that within the term *uncertainties* there are numerous independent sources of uncertainties, such as flow rates and pressures. For our applications, they consist of chemical purities, flow rates, pressures, and temperature readouts. The uncertainty analysis herein nests the related parameters together to get a global uncertainty for the concentration that may be applied to the cross-section measurements, using the RSS method (Equation 1).

For an uncertainty analysis within absorption spectroscopy and quantification of species from the JSR, there are several aspects that must be taken into account. First, the Arrhenius equation is exponentially dependent on temperature, so it is important to be able to know the temperature inside the JSR to represent the data accurately. The Arrhenius equation (Equation 3a) provides a quantification of the reaction rates based on their temperature dependence. In the Arrhenius equation, A is a pre-exponential factor that includes the frequency of collisions in the correct orientation, E_a is the activation energy, and k_B is the Boltzmann constant. Equation 3b is a modified form of Equation 3a, and includes a power, n , to the temperature ratio, $T/298$, to capture non-linear temperature dependence of the pre-exponential factor. Figure 6 contains an example where the exponential dependence is displayed numerically from the decomposition reaction of H_2O_2 .

$$k = Ae^{\frac{-E_a}{k_B T}} \quad (3a)$$

$$k = A \left(\frac{T}{298} \right)^n e^{\left(-\frac{E_a}{R_u T} \right)} \quad (3b)$$

$H_2O_2 \xrightarrow{k} \dot{O}H + \dot{O}H$							
	A	Ea (kJ/mole)	R (kJ/mole*K)	T (K)	n		
	6,90E-04	219	8,31E-03	298	-4,57		
T=	800	805	810	825	850	900	
k (T) =	3,80E-20	4,53E-20	5,39E-20	8,96E-20	2,00E-19	8,61E-19	$cm^3 / molecule * s$
k(T)/k(800)=		19%	42%	136%	426%	2165%	

Figure 6: Application of the Arrhenius equation to the decomposition reaction of hydrogen peroxide to form hydroxyl radicals [4].

Using values obtained by Sellevag et al. [4], calculations of the rate coefficients for 800 K were produced from the decomposition reaction of H_2O_2 , in addition to the inclusion of increments of 5, 10, 25, 50, and 100 K, respectively, to demonstrate the effect of different temperatures. Figure 6 contains the calculated values, and based on the investigated reaction, a difference of 5 K induced approximately a reaction rate that was 1.19 times faster, and as much as 22.6 times faster with a difference of 100 K. This is important for combustion applications because how quickly a reaction occurs will greatly affect its feasibility. If the reaction is too slow at a prescribed temperature, the reaction might not have sufficient time to occur inside the piston cylinder of a car during its cycle.

Second, it is important to investigate whether a thermal gradient will be induced inside the JSR, as a uniform temperature is an underlying assumption that needs validation. This is what the focus of the present work is meant to quantify. After the measurements were taken, it became apparent that there was a thermal gradient inside the JSR, and the temperature was at its highest in the center of the reaction volume of the

JSR, and decreased as it became closer to the throat of the JSR nozzle. This was true for all flow rates and heating temperatures tested, which illustrates how consistent the JSR is over a large range of temperatures. This is important because it encapsulates what the temperatures most likely are at any point along the transversal axis on which the sampling probe and thermocouple traverse. Figure 7 contains a general temperature vs. distance plot, illustrating the trend that was observed. The set temperature is the temperature the reactor was set to operate at, as measured by the thermocouple. Actual temperature is what the thermocouple was reading at a given location inside the reactor. The temperature gradient is the ratio of the change in temperature over the change in distance traversed.

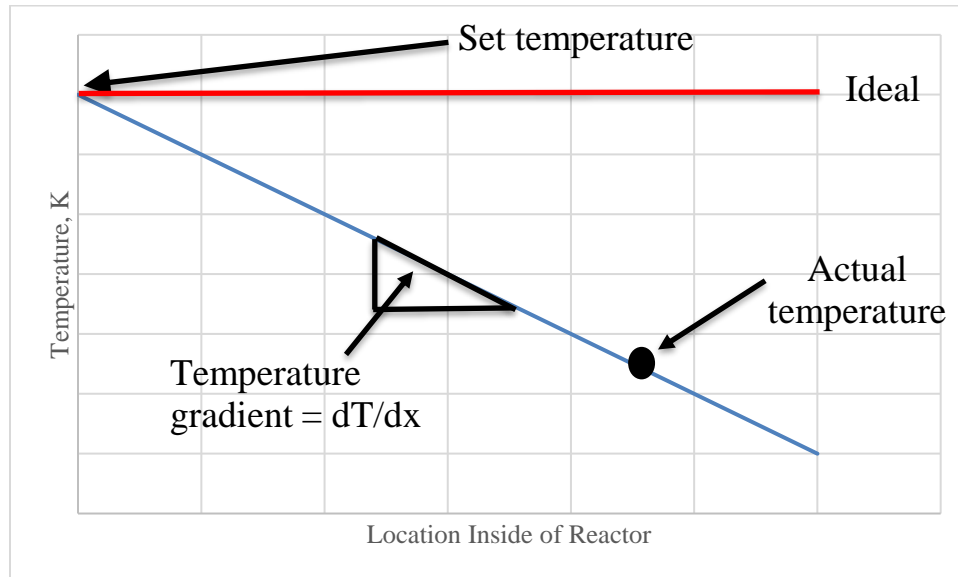


Figure 7: Generic plot of temperature as a function of the location inside the reactor. Set temperature is the temperature the reactor was set to operate at. Actual temperature is what the temperature is at for a given location inside of the reactor. Temperature gradient, dT/dx , is the ratio of the change in temperature over the change in distance traversed. Ideal is when there is no gradient present.

CHAPTER 2

BACKGROUND

Accounting for uncertainties in laboratory experiments is a rigorous study. Uncertainty refers to the improbability that a measurement point will fall within the probability distribution of measurements. For engineering, it is common for data to follow a *normal* distribution, which is often called *Gaussian distribution*. Gaussian distribution represents the range within the data falls within. For applications in combustion experiments, it is imperative that a rigorous analysis is conducted, due to the nature of tight tolerances on chemical kinetics. Combustion chemistry, specifically chemical kinetics, is exponentially dependent on temperature. The Arrhenius equation (Equation 3a&3b) is used to calculate reaction rates for a species, which is a means to measure how fast a certain reaction occurs. The application of the Arrhenius equation is crucial in combustion applications because of its temperature dependence, which emphasizes further importance on tracking uncertainties that accumulate. For internal combustion engine applications, it is imperative to associate reaction temperatures with reaction conditions, specifically temperature and pressure. It is important because of the ignition properties. For a fuel to ignite, it must reach a certain temperature, pressure, and sufficient oxygen. When this is applied to internal combustion engines, inherently it will be time dependent also.

As the sole purpose of a JSR is to study chemical kinetics and the products of formation and their concentrations from a chemical reaction in a steady state turbulent

flow reactor, it is imperative to introduce fluid mechanics in addition to chemistry. Fluid mechanics become important as it governs the residence time inside the reactor, which is analogous to a piston/cylinder inside an internal combustion engine. Adjusting the residence time via adjusting the volumetric flow rate provides for greater control over the reaction conditions. It is important to analyze how fuels combust and decomposes while exposed to oxygen for different lengths of time. It is not until such an analysis is conducted that conclusions can be drawn as to what is produced and its quantity. Given the overview of the importance of combustion experiments, it can be deduced that to control the experimental environment as good as possible, it is crucial to be able to quantify every measurement, and knowing its uncertainty. Providing an uncertainty analysis increases the credibility of the study as it takes pride in knowing the unknown. This is also important because it can introduce specific sources of error that could be produced, and provide a means to improve them.

Several research groups use jet-stirred reactors (JSR) for combustion studies: Princeton University [5], CNRS-Orléans [6], and CNRS-Nancy [7]. While they all feature a JSR, there are differences in the sampling procedure. The sampling procedure at the University of Georgia is most similar to the setup at CNRS-Orléans, with the use of a sonic sampling probe to extract the sample from the reaction volume [6]. At CNRS-Nancy, molecular beam mass spectrometry is used rather than sonic probe sampling to extract gaseous sample and temperature profiles are not measured due to hardware limitations. The CNRS-Nancy setup uses online analysis as the outlet of the reactor is directly connected to chromatographs with three columns (carbosphere packed column,

PlotQ capillary column, and a HP-5 capillary column), a TCD (thermal conductivity detector), and an FID (flame ionization detector) [6].

To date, no rigorous experimental uncertainty analysis has been conducted for JSR applications, but rather assumptions on individual equipment, and not on the global scale.

Karsenty et al. [8] reported an approximated uncertainty in species concentration of $\pm 15\%$, reactor temperature of $\pm 5\text{K}$, and residence time of $\pm 0.02\text{s}$, but no reference as to how the numbers were achieved. Serinyel et al. [9] reports an estimated global uncertainty of 1.5%, while not providing an analysis or any reference to how the global uncertainty is reached. Song et al. [7] provides separate uncertainties of the equipment used but also lacks a deeper investigation into providing a global uncertainty for the measurements obtained using the JSR. Song provides a global uncertainty of $\pm 5\%$, which is an estimate, for all diagnostic instruments, while an uncertainty of $\pm 10\text{-}15\%$ for two other instruments. Bugler et al. [6] follows suit via only listing individual uncertainties rather than investigating it further and representing the global and propagated uncertainty. The JSR setup at CNRS-Nancy does provide a numerical value for a temperature gradient inside the reaction volume, and lists it as less than 5 K but with no reference to which unit of length [6]. CNRS-Orléans has a sonic probe with a fused-silica protected thermocouple that can be moved along the reactor center line to verify thermal and concentration homogeneity [10]. However, Burke et al. [10] does not reference a study that provides a detailed description that supports the claim of thermal and concentration homogeneity. A study to verify the thermal homogeneity is precisely what is conducted in this present work across a range of temperatures and residence times.

CHAPTER 3

METHODOLOGY FOR UNCERTAINTY QUANTIFICATION

Mass Flow Controller Uncertainty Analysis

Mass flow controllers (MFC) from Bronkhorst operate via thermal conductivity with the use of temperature sensors. Gases – as do all matter – have some value of thermal conductivity, which is a physical property of matter that relates to the rate at which heat passes through the matter. Inside of a MFC is a heated filament that is connected via circuitry to temperature sensors. The amount of heat removed from the filament corresponds to a certain amount of mass passing over it, as expressed in Equation 4.

$$d\dot{Q} = \dot{m}c_p dT \quad (4)$$

The mass flow rate is determined by (a) knowing the gas composition, thus c_p , and (b) the dT measurement by the sensors. The heat transfer is determined by the amount of electrical current that the filament requires. A flow splitter will be actuated to maintain the requested flow rate. As moving parts wear down over time due to mechanical fatigue, it is important to have a means to validate the reliability of equipment and make periodic inspections. Combustion experiments rely heavily on the accuracy of MFCs, which deliver oxygen, nitrogen, and other gases to chemical reactors at specific flow rates. Bounds of uncertainty within flow controllers can lead to inaccurate control of gas flow and can introduce systematic error. Flow controllers with a large operating full-scale range may operate with a non-linear behavior near upper and lower limits. Determining

the bounds of uncertainty of the flow controllers will create the foundation for in-house calibration and future experiments. Currently there are no solutions on the market to check the calibration of MFCs, but if there were any, they would undoubtedly be very expensive. An in-house alternative will save costs in addition to provide a deeper understanding into the equipment's use and functionality. The in-house solution consisted of one setup that was identical each experiment, except for the MFC, as that is what is being studied. The investigation was conducted by using a series of known internal volumes, a pressure gauge, a mass flow controller, compressed gas, and a vacuum system, as laid out in Figure 8. Table 1 contains all parts that were subjected to exposure by the gas used.

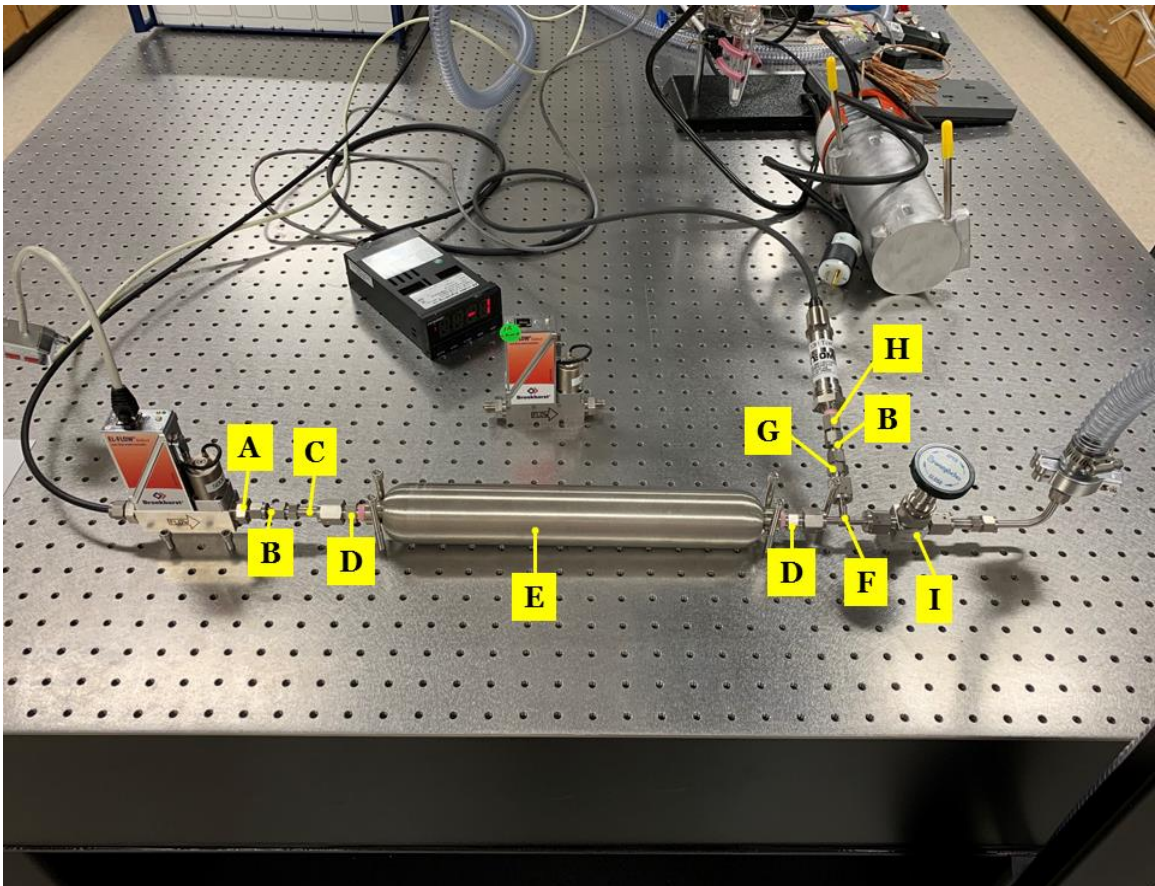


Figure 8: The experimental setup for the MFC uncertainty analysis. Each letter labels individual parts which contribute to the overall internal volume that must be accounted for.

Table 1: Summary of all wetted parts for calculation of internal volumes. Labels correspond with the part as labeled in Figure 8.

Label	Part Number	Internal Diameter/Length (cm ³)	Internal Volume (cm ³)	Notes
A	(see drawing)	0.23/0.40 in	0.2720	
B	SS-401-PC	0.1695/0.985 in	0.3638	Port Connector - Fractional
C	SS-4-WVCR-6-400	0.1795/1.65 in	0.6096	Tube Fitting Connector
D	SS-4-VCR-1-4	0.1795/1.49 in	0.5506	Male NPT Connector
E	304L-HDF4-500-T		500	Sample Cylinders
F	6LV-4-WVCR-T-FFF	0.1735/0.4885(3) in	0.5637	VAR Welded VCR Face Seal Fitting, Female Tee (N/A)
G	SS-4-VCR-6-400	0.1755/1.33 in.	0.5260	Tube Fitting Connector
H	SS-400-7-2	0.1900/0.789 in	0.3654	Female Connector (Tapered Thread) - Fractional
I	SS-4BG-VCR	0.1875/2.058 in	0.9308	Stainless Steel Bellows Sealed Valve (N/A)

The analysis was performed on four different Bronkhorst MFCs: 50 sccm O₂, 50 sccm N₂, 500 sccm O₂, and 5000 sccm N₂. For each MFC, a desired flow rate was set on the computer software, then recorded the time it took to reach a steady state pressure value using a stop watch. Once a steady pressure had been reached, the pressure was also documented in addition to the time it required. The study was to be conducted on flow rates from 1% to 100% of the full-scale. The objective was to encapsulate twelve different data points, working from 1% all the way to 100%, and then back down to approximately 2%. This was done by taking six separate set values between 1% and 100% and relatively spaced out. The operation then proceeded from 100% down to 2% of

the full-scale, with slightly different percentages of the full-scale to check linearity and get data points that would not be on the same requested flow rate. Table 2 provides an example of the incremental strategy, with this table dedicated to a 50sccm O₂ MFC.

Table 2: Data set with requested flow rates in the left column, where the incremental strategy is displayed.

Set Flow Rate (sccm)	Δt (min)	Pressure (Torr)	Actual Flow Rate (sccm)
0.50			
2.00			
15.00			
28.00			
37.00			
50.00			
44.00			
31.00			
19.00			
10.00			
4.00			
1.00			

The actual flow rate was calculated using Equation 5, where known values or parameters that are measurable, such as pressure and time are inserted. Temperature was assumed to be constant for all experimental trials. Equation 5 is derived from the ideal gas law. To calculate the volumetric flow rate, a known volume of substance must be added per unit time, hence dV/dt . This can be achieved via rewriting dV/dt , namely quantifying (a) the

number of particles (colloquial term for atoms or molecules) of a species per unit time, and (b) quantifying the volume per number of particles, called molar volume, at standard conditions. Multiplying (a) and (b) will yield volumetric flow rate. (a) can be rewritten using the ideal gas law solving for an expression for N, the number of moles, which yields PV/RT. This is useful because now the equation contains pressure, which is a parameter that can be physically measured via pressure transducers. The rewritten portion is then divided by the time it required to reach a steady pressure reading, and finally multiplied by (b) to arrive at Equation 5.

$$\dot{V}_{actual} = \frac{V}{\Delta t} = \left(\frac{N}{\Delta t}\right) \left(\frac{V}{N}\right) = \left(\frac{PV}{R_u T}\right) \left(\frac{1}{\Delta t}\right) \left(\frac{V}{N}\right) \quad (5)$$

The reason for the uncertainty analysis on the MFCs was to ensure they operate in a linear fashion across their entire flow rate span. As with most equipment, the quality of moving parts worsens over time, and to ensure the flow controllers still operate at the prescribed flow rates, this analysis will be very crucial to perform periodically. Measurements are only as accurate as the equipment. The setup in Figure 8 is a permanent fixture, with an internal volume of 505 cm³, and can be used for all of the Bronkhorst MFCs that are present in the combustion laboratory at the University of Georgia, allowing for a quick hookup and analysis. Another advantage of the permanent affixture is that it will always the same parts and configuration, making comparisons comparable from previous analyzes. As the system is vacuumed prior to each run, there is no need to worry about contamination from other gases; however, the only MFCs that are in operation in the reactor setup are N₂ and O₂, with separate gas lines that are hooked up to the MFC. This setup will inherently incur errors, as the time recorded also accounts for

gases to travel in the gas lines, response time, and MFCs to reach steady state. However, as this setup will be used multiple times, it serves as a datum to reference future calibrations to.

Cross-Section Measurements Uncertainty Analysis

Cross-section measurements are obtained using a vacuum ultraviolet spectrometer, which produces absorbance (I/I_0) as a function of wavelength, and, as species have species-specific absorption features, it makes the process of analyzing species from a mixture a possibility. Provided the parameters of interest for absorption spectroscopic measurements in the VUV, it is of interest to analyze the effects of uncertainty on absorbance, which has proportional relationship to the concentration in Beer-Lambert's Law, depicted in Equation 2. However, a modified Beer-Lambert's Law is used in spectroscopy, and is provided in Equation 6. In Equation 6, σ is the cross-section of the species, c is the concentration, and L is the path length.

$$\log_{10} I_0/I = \sigma c L \quad (6)$$

This is especially important when assessing the products formed in combustion experiments. Cross-section measurements serve to identify species. An uncertainty analysis was conducted for the cross-section measurements. The calculated uncertainty was based on the root-sum-squares (RSS) method. It is a method that is commonly used in uncertainty calculations when analyzing one variable and serves as a mean to quantify error propagation. In combustion experiments, it is of interest to assess the uncertainty in the concentration, which in turn comes from Dalton's law of partial pressures. The uncertainty is to be calculated for our chemical mixtures, which are created in a separate

manifold. The measurement largely consists of three pressure gauges, which are used for measurements of pressure exerted by the vaporized chemical, pressure exerted by the inert gas (He), and downstream to regulate the pressure going into the VUV apparatus. Even the best of pressure gauges come with inherent uncertainties. Table 3 compiles the devices used in the manifold and their associated uncertainties.

Table 3: Compiled list of the instruments in the manifold uncertainty calculations.

Device	Manufacturer	Measured Property	Error
Capacitance Manometer	MKS	Pressure (0-10Torr)	$\pm 0.12\%$ of P
Capacitance Manometer	MKS	Pressure (0-5000Torr)	$\pm 0.12\%$ of P
Capacitance Manometer	MKS	Pressure (0-1000Torr)	$\pm 0.25\%$ of P

As the mixture process is comprised of two stages, we have to separate them into two separate RSS evaluations. First stage is the manifold, in which the chemical is vaporized and collected in a cylindrical tank, which is in vacuum. The pressure exerted in the cylinder by the chemical is measured and noted. Then, an inert gas (He) is added to the tank, diluting the chemical composition, and total pressure is measured and noted. The second stage is connecting the tank to the setup that enters the spectroscopic device, with a pressure flow controller to maintain a set pressure. The two separate RSS evaluations are for each stage, respectively. For stage 1, it needs to be broken into two parts due to two pressure readouts.

- a) (chemical impurity)*(measured pressure)*(the uncertainty listed in the data sheet for the pressure transducer).
- b) (total pressure value)*(the uncertainty listed in the data sheet for the pressure transducer).

a) and b), respectively, are then applied to the RSS method in Equation 1. u_1 is the value obtained from (a), and u_2 is the value obtained from (b). For stage 2, the RSS method on one number just yields the uncertainty, u_3 , alone from the datasheet, since it takes the square root of a square. These calculated uncertainties are in units of pressure (Torr). To apply this to the VUV spectra, it would be preferred to represent the uncertainty in percent. This is converted using Equation 7. With all u_k in terms of percentages, the overall uncertainty, u_{ab} , is then calculated via application of Equation 1.

$$\text{uncertainty \%} = \frac{\text{uncertainty in Torr}}{\text{total pressure in Torr}} * 100 \quad (7)$$

For the stage 2, the RSS method yields a percent value equal to that of the uncertainty listed in the datasheet, since it takes a square root of a square, u_c . To get a final value on the entire measurement, a RSS evaluation is calculated on the squares of the uncertainties, u_k , from stage 1, stage 2, and the chemical uncertainty, respectively. This uncertainty is then accounted for in the cross-section measurements. Equation 8 provides a visual representation of the RSS method for the application to the setup studied herein. Each stage in the equation corresponds to the uncertainty in % for that stage.

$$\text{Overall uncertainty (\%)} = \sqrt{u_{ab}^2 + u_c^2 + (\text{chemical impurity})^2} \quad (8)$$

Jet-Stirred Reactor Uncertainty Analysis

To obtain experimental data on the JSR, a linear motion thimble that translates rotational movement into linear movement is used, and is shown in Figure 9. A thermocouple was connected to the thimble, enabling the possibility to take temperature readings at various locations inside of the JSR.



Figure 9: Linear motion thimble. It is mounted onto the reactor and the probe is attached inside of it, allowing it to traverse along the horizontal plane.

A total of 20 data points were taken in each direction, divided into even increments between the center of the reaction volume ($x = 0$ cm) and the throat of the converging-diverging nozzle ($x = 3.00$ cm). Figure 10 illustrates the placement of the thermocouple and its directional degrees of freedom, as well as the location of the converging-diverging nozzle. Each data point took requires minutes (per time study in Figure 13), making each set of 20 data points require approximately 3½ hours, and an equal amount of time to capture the reverse direction.

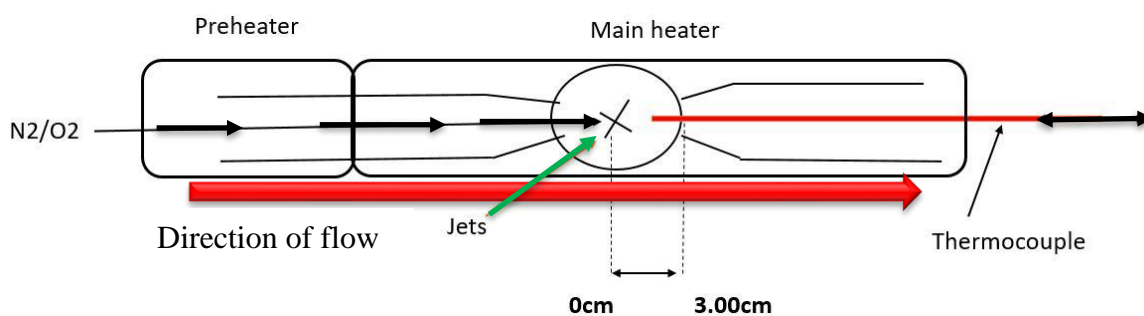


Figure 10: Schematic of the jet-stirred reactor, indicating the center position ($x=0.00$ cm), and the location of the throat ($x=3.00$ cm). Thermocouple can be horizontally translated via a rotational-to-linear thimble. The reaction volume is depicted as a circular sphere with an internal volume of 30cm^3 .

Figure 11 illustrates the positioning of the reaction volume inside the reactor housing, and Figure 12 provides a top view of the reactor housing, where the yellow shade provides the location of the preheaters (left), and preheaters (right).

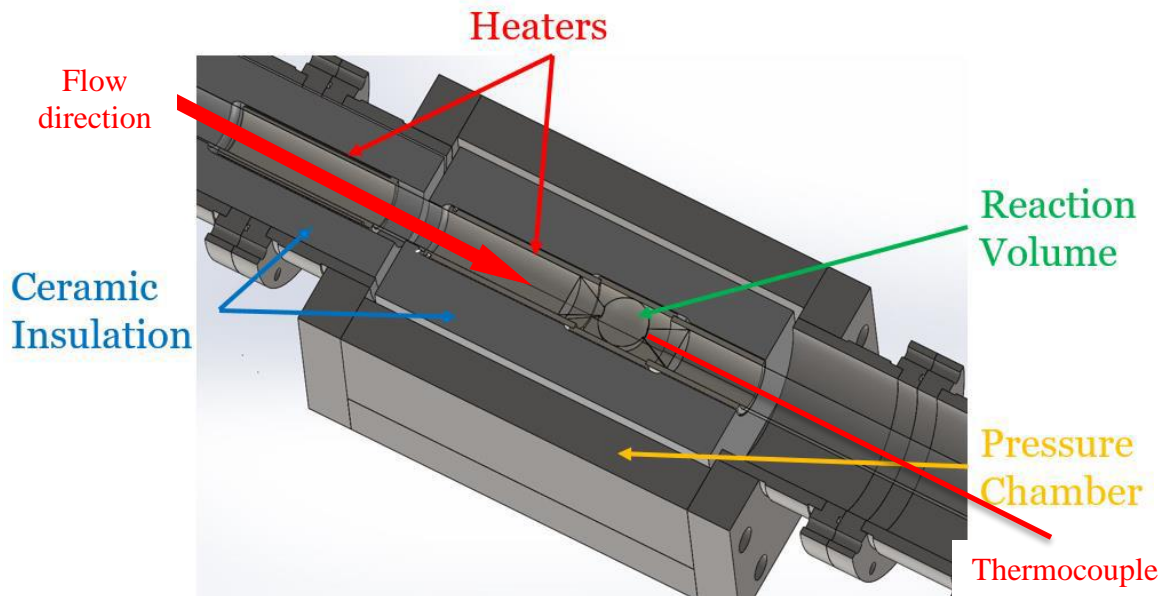


Figure 11: The placement of the reaction volume and its location in relation to the preheaters and main heaters. The red line is the thermocouple. Flow occurs from left to right.[3]

The increments were $1.5 \text{ mm} \pm 0.1 \text{ mm}$, allowing to work within the accuracy of the thimble, which is accurate to 0.1 mm. It was important whilst taking these measuring points to allow adequate time for the thermocouple to reach a steady value, which was estimated to be approximately ten minutes. To confirm that the timescale was sufficient, a time study was conducted where each temperature for each time measurement was recorded after repositioning the thermocouple, illustrated as the red line in Figure 10. The time study was conducted at $x = 2.05 \text{ cm}$ when relocated from $x = 1.89 \text{ cm}$ at a temperature of 227°C (500 K) for the main heater and preheater, with a residence time of 1000 ms. This was compiled into a plot, which is in Figure 13.

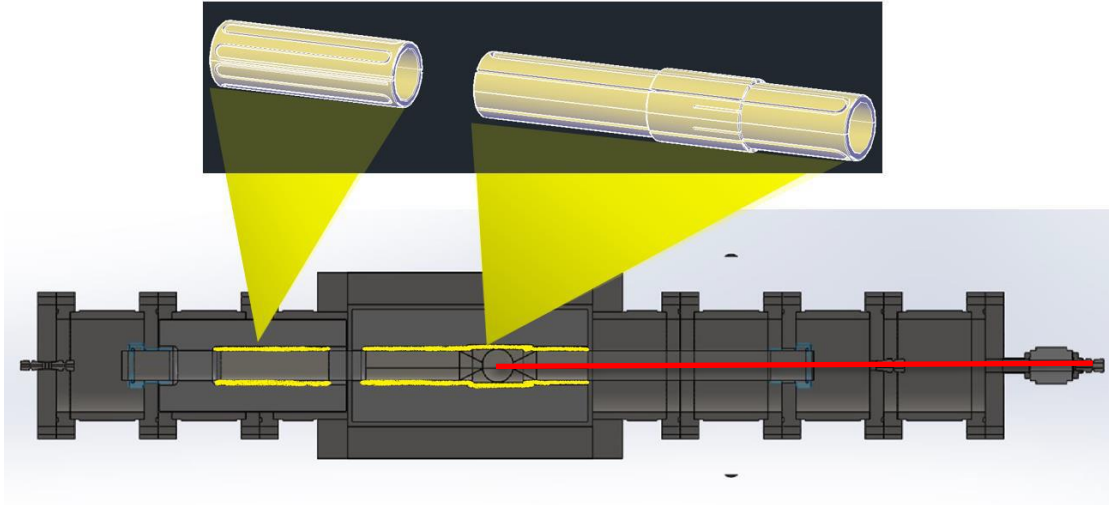


Figure 12: Location of the preheater (left) and main heater (right) relative to the bulb of the jet-stirred reactor. Red line is the thermocouple.[3]

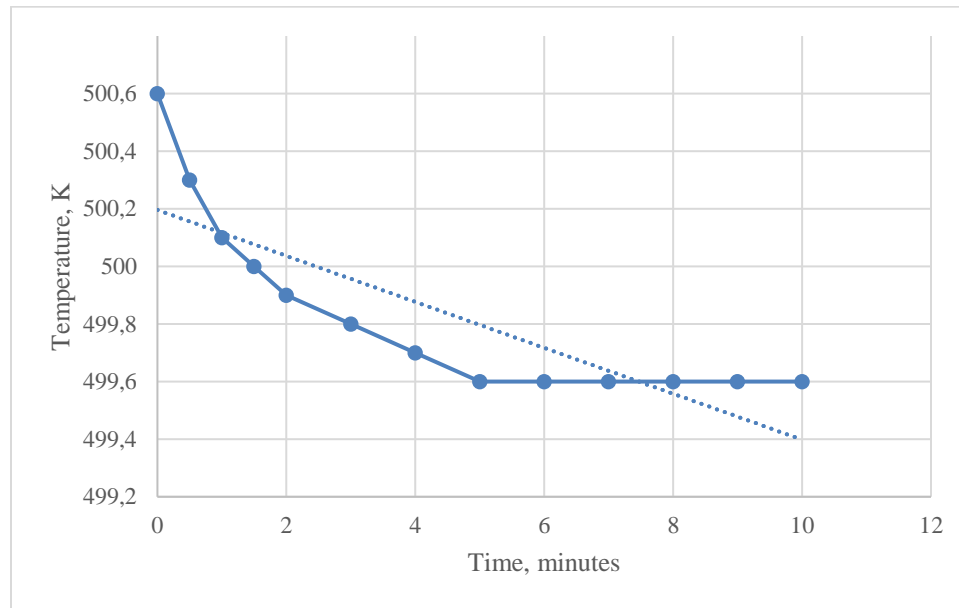


Figure 13: Plot of the time study conducted at $x=2.05\text{cm}$ for a reactor temperature of 500 K, preheating temperature of 500 K, residence time of 1000 ms. At time 0 the thermocouple was displaced from $x = 1.89\text{ cm}$ to $x = 2.05\text{ cm}$. A ten minute period to allow the thermocouple to equilibrate to the new environment is sufficient.

As Figure 13 suggests, a waiting time of ten minutes is more than sufficient to allow the thermocouple to stabilize to the new environment, and provide readings accurate to within the uncertainty bounds of the thermocouple, which is $2.2\text{ }^{\circ}\text{C}$ at a reactor temperature of 500 K.

As low temperature combustion (LTC) can be considered for the region of 500-1200 K, it was suitable to analyze the lower and upper bound, respectively, in addition to a value in the middle, which was chosen to be 750 K. Due to the design of the preheaters, its maximum temperature is 800 K, so a choice of 750 K as a middle ground seemed appropriate to analyze the temperature gradient, dT/dx , for the case when the reactor temperature matches that of the preheater. The maximum temperature for the main heaters is 1250 K, so that is why a temperature of 1200 K was selected. A total of 60 measurements were taken, as labeled in Table 4, with 30 in each translational direction to check for validation of repeatability. This was performed by taking measurements at 20 different locations downstream (forward), and concluded going upstream (backward), while recording the temperature readings at the same locations. Each empty cell in Table 3 required approximately 3½ hours to complete.

Table 4: Test matrix for the experiments that were conducted, where the empty cells are populated after each experimental run. This was applied for the downstream and upstream translational directions, respectively. Cells that would result in duplicate runs due to preheater temperature exceeding desired set point, even when turned off, are labeled N/A.

Preheater temperature(K)	Residence time (ms)	dT/dx ($T_R = 500$ K)	dT/dx ($T_R = 750$ K)	dT/dx ($T_R = 1200$ K)
Turned off	500			
	1000			
	2000			
373	500			N/A
	1000			
	2000			
500	500			N/A
	1000			
	2000			
973	500			
	1000			
	2000			

The process is illustrated later, in Figure 19, with the black arrows. Measurements for the reactor temperature of 1200 K with preheating at 373 K and 500 K, respectively, could not be obtained as the radiative heat transfer from the main heaters caused the preheaters to reach a temperature of 512 K for the first study when preheaters were turned off. The respective cells in Table 3 are labeled N/A. This would only create duplicate runs, twice. Full analysis of this will be included in Chapter 4, but a summary of the trends is provided in Table 5. In general, when the preheating temperature was held constant and reactor temperature increased, the dT/dx would increase for a given residence time. The same was observed for the case when the reactor temperature was held constant and the preheating temperature was increased.

Table 5: Trends in a summarized and tabulated form from populating Table 4.

Residence Time	Pre-Heater Temperature (K)	Reactor Temperature (K)	dT/dx
500 ms	Constant	Increasing	Increase
	Increasing	Constant	Increase
1000 ms	Constant	Increasing	Increase
	Increasing	Constant	Increase
2000 ms	Constant	Increasing	Increase
	Increasing	Constant	Increase

CHAPTER 4

UNCERTAINTY MEASUREMENTS

Mass Flow Controllers

A thorough investigation was done on the mass flow controllers used in the laboratory. This was conducted with an undergraduate student, Dylan Brown, whom I mentored, and was sponsored by CURO (Center for Undergraduate Research Opportunities). The goal was to quantify the accuracy of the mass flow controllers and validate the assumption that the MFCs are accurate along the entire full-scale range. The result of these experiments was a plot for each of the mass flow controllers, plotting the requested volumetric flow rate against the actual flow rate, and were indeed very linear, with R^2 values of 0.9999 or higher.

Figures 14-17 provide the results obtained from the experiments on the MFCs studied. However, it is expected that the actual results are much better. Included in Figures 14-17 is a trend line whose slope is 1 and intercept is 0, which is what is expected. The method to obtain the volumetric flow rates inherently had unavoidable errors that could not be improved, and should be taken into consideration when evaluating the data. The errors that were unavoidable were the time required for the volumetric flow rate to equilibrate, and time required for the pressure to equilibrate. However, the trend lines indicate the entire full-scale range is operating in a linear fashion, which is of utmost importance for combustion experiments requiring a wide range of flow rates. It validates the assumption that the flow controllers are very accurate,

and equally accurate along their full-scale range, especially at the lower end of the range where more data points were collected.

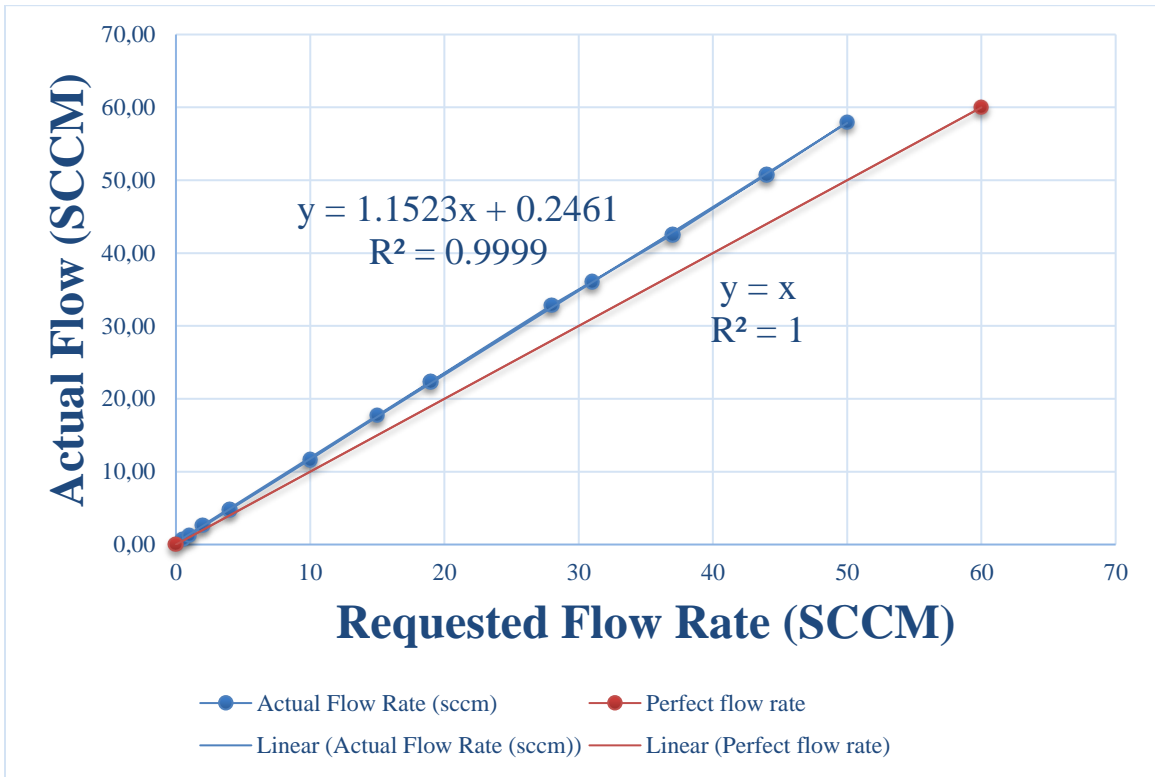


Figure 14: Flow rate experiment for 50 sccm O₂ mass flow controller.

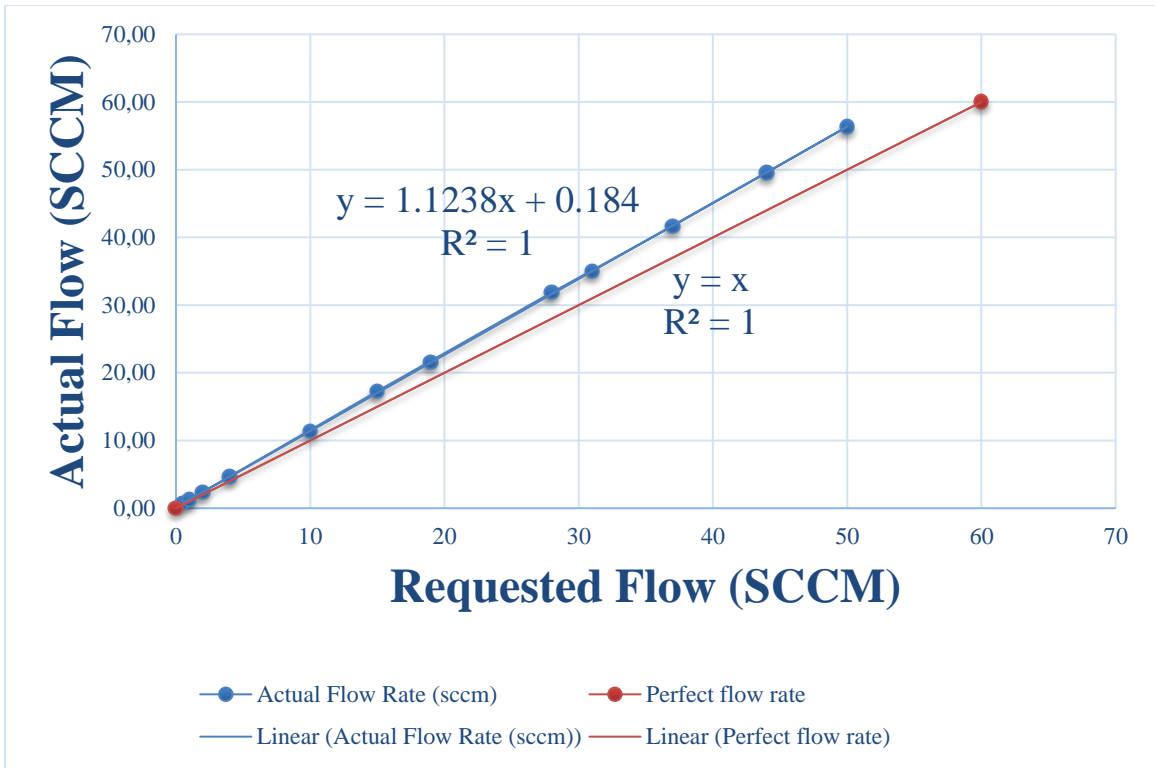


Figure 15: Flow rate experiment for 50 sccm N₂ mass flow controller.

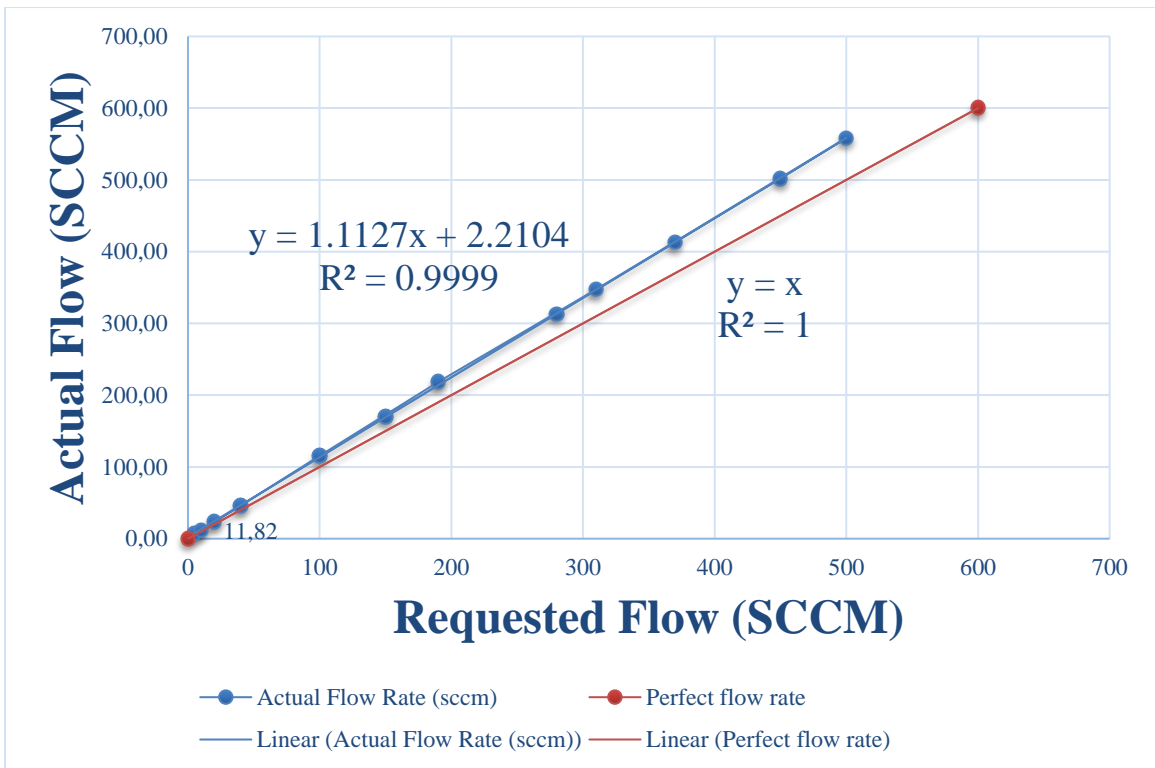


Figure 16: Flow rate experiment for 500 sccm O₂ mass flow controller.

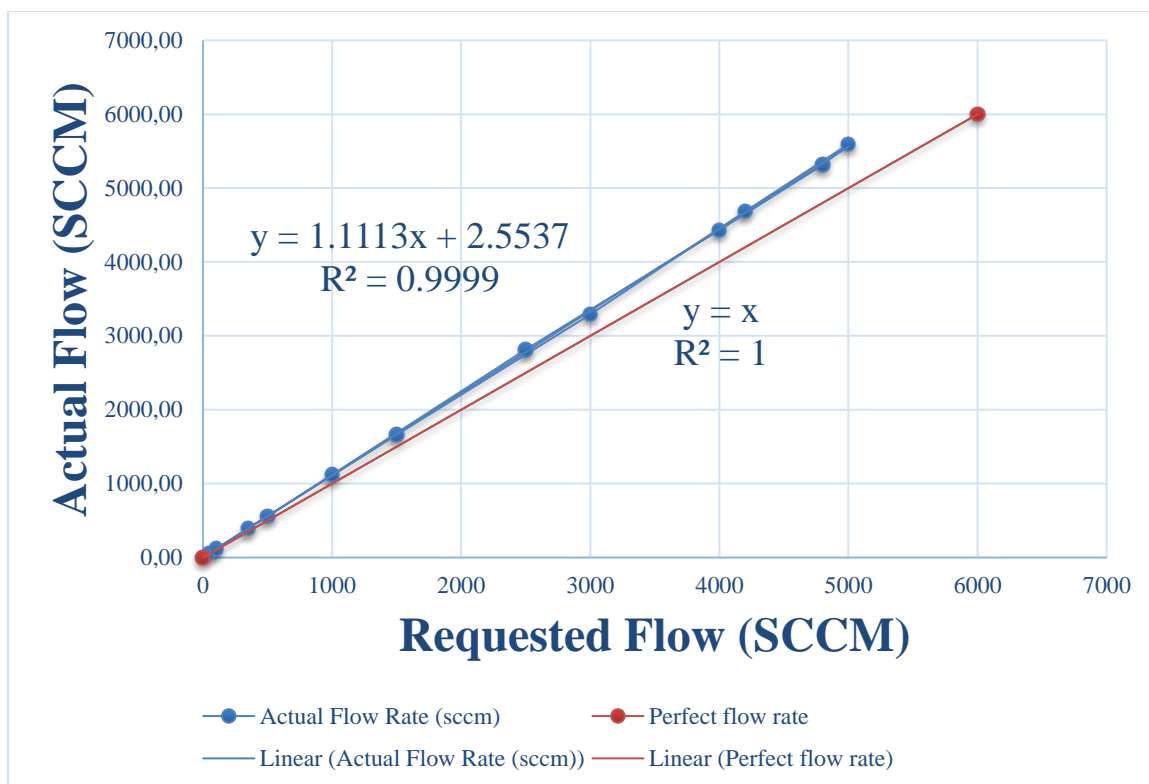


Figure 17: Flow rate experiment for 5000 sccm N₂ mass flow controller.

Cross-Section Measurements

An uncertainty analysis was conducted on the cross-section measurement setup, which includes a chemical mixing manifold station, sampling station, and the VUV absorption diagnostic. The extensive research that went into the propagation of errors was implemented into a Microsoft Excel spreadsheet, while including mathematical logic to conduct the numerical analysis. The values of partial pressures are entered into the orange cells in Figure 18. As mentioned in Chapter 4, the *final uncertainty* was calculated using the RSS method based on the values in cells F7 and I5, respectively. The uncertainty is to be implemented in representation of the cross-section graphs, which visualize the absorption of the species as a function of wavelength. An example of the application to graphs can be found later, in Figure 43, visualizing an uncertainty of $\pm 5\%$. This is useful

because it provides an increased in-depth understanding of what contributes to overall uncertainty and its impact in the end-product.

	A	B	C	D	E	F	G	H	I
1	Uncertainty for VUV								
2									
3									
4	Chemical purity (%)	0-10 Torr readout (Torr)	0-10 Torr uncertainty (Torr)	5000 Torr readout (Torr)	5000 Torr uncertainty (Torr)	Mixture uncertainty (Torr)	VUV pressure readout (Torr)	VUV pressure uncertainty (Torr)	Cell uncertainty
5	98	0,802	0,000019248	4026	4,8312	4,83	800	2	0,25
6									^ is in percent
7						0,12			
8	Inputs					^ is in percent			
9									
10	Final calculation								
11									
12			Final uncertainty						
13			2,02	%					

Figure 18: Screenshot of the uncertainty calculator created for the chemical mixture and VUV setup. Orange cells are entered manually with the partial pressures from the mixture stage. The gray cells contain the calculated uncertainties.

JSR Temperature Measurements

The results from the JSR measurements were compiled into a Microsoft Excel spreadsheet. Figure 19 provides an example of one of 500 K experimental runs. A total of 20 measurements were taken, in each translational direction, to assess hysteresis error, which is the error that results from different outputs (temperature) to the same input (location of the thermocouple). This was done for all cases as listed in Table 4, namely for three different reactor temperatures of 500 K, 750 K, and 1200 K. At each reactor temperature, a temperature gradient, dT/dx , was calculated for different preheating temperatures and residence times. Figure 19 is a fully populated Table 4, where F indicates forward (downstream) direction, and B indicates backward (upstream) direction.

Table 6: Final compilation of the test matrix (table 3) with the calculated dT/dx values obtained from individual experiments, as shown in figure 16. The experiments were conducted in the downstream (forward) direction and upstream (backward) to encapsulate hysteresis error. F indicates forward (downstream) direction; B indicates backward (upstream) direction.

Preheater temperature(K)	Residence time (ms)	dT/dx (K/cm) (T _R =500 K)		dT/dx (K/cm) (T _R =750 K)		dT/dx (K/cm) (T _R =1200 K)	
		F	B	F	B	F	B
Turned off	500	-0.40	-0.73	-3.33	-3.57	-6.07	-6.63
	1000	-1.77	-2.07	-5.07	-5.30	-9.90	-9.30
	2000	-1.97	-2.47	-5.13	-5.70	-10.63	-11.47
373	500	-0.87	-0.63	-4.77	-3.20	N/A	
	1000	-2.50	-2.57	-5.10	-5.83		
	2000	-3.17	-3.67	-5.83	-6.93		
500	500	-2.17	-2.27	-4.60	-5.17	N/A	
	1000	-3.83	-4.03	-6.33	-6.47		
	2000	-3.70	-4.57	-5.73	-6.13		
973	500	-6.87	-7.93	-8.00	-8.10	-9.57	-11.77
	1000	-6.73	-7.33	-7.20	-7.60	-10.97	-11.20
	2000	-6.87	-6.90	-9.70	-8.07	-10.77	-10.30

NO PRE-HEATER Forward				NO PRE-HEATER Backward			
T _{probe} (°C)	T _{forward} (K)	dT (K)	x (cm)	T _{probe} (°C)	T _{backward} (K)	dT (K)	x (cm)
188,3	461,3		0,00	186,7	459,7		0,00
188,6	461,6	0,3	0,16	186,9	459,9	0,2	0,16
188,7	461,7	0,1	0,32	187,2	460,2	0,3	0,32
188,8	461,8	0,1	0,47	187,5	460,5	0,3	0,47
188,8	461,8	0	0,63	187,8	460,8	0,3	0,63
188,8	461,8	0	0,79	188,3	461,3	0,5	0,79
188,9	461,9	0,1	0,95	188,5	461,5	0,2	0,95
189	462	0,1	1,11	188,7	461,7	0,2	1,11
189,2	462,2	0,2	1,26	188,9	461,9	0,2	1,26
189,2	462,2	0	1,42	188,9	461,9	0	1,42
189,2	462,2	0	1,58	188,8	461,8	-0,1	1,58
189,1	462,1	-0,1	1,74	188,6	461,6	-0,2	1,74
189,1	462,1	0	1,89	188,3	461,3	-0,3	1,89
188,9	461,9	-0,2	2,05	188,3	461,3	0	2,05
188,8	461,8	-0,1	2,21	188,4	461,4	0,1	2,21
188,7	461,7	-0,1	2,37	188,3	461,3	-0,1	2,37
188,7	461,7	0	2,53	188,3	461,3	0	2,53
188,5	461,5	-0,2	2,68	188,2	461,2	-0,1	2,68
188,2	461,2	-0,3	2,84	188	461	-0,2	2,84
188	461	-0,2	3,00	188	461	0	3,00
minimum (K)	462,2			minimum (K)	461,9		
minimum (K)	461			minimum (K)	459,7		
dT/dx (K/cm)	0,40			dT/dx (K/cm)	0,73		
average (K)	462			average (K)	461		
standard deviation (K)	0,3			standard deviation (K)	0,6		

Figure 19: Example of the sampling experiment for a reactor temperature of 500K prior to gases flowing, and with the preheaters turned off.

The preheating temperatures investigated at were with the preheaters turned off, at 373 K, 500 K, and 973 K. The residence times investigated were 500 ms, 1000 ms, and 2000 ms. As concluded from the time study, each temperature reading was allowed approximately ten minutes to equilibrate. The thermocouple is a K-type, which consists of Nickel-Chromium / Nickel-Alumel alloy. A K-type thermocouple was used because its temperature range is 0-1100°C, and the maximum temperature the reactor can achieve is 1200 K (927°C).

A consistent trend was observed, namely that the temperature decreased the further the thermocouple was from the center of the reaction volume. In Figures 20-28, plots are produced that illustrate the trends as a function of the location of the thermocouple. Each figure has an associated table (Tables 7-15) that contains the trend lines that were computed, and their associated R^2 value. The linear regression value, R^2 , is a measurement of how well data fits a trend line. An R^2 value ranges from 0 to 1, where a value of 1 indicates a perfect fit.

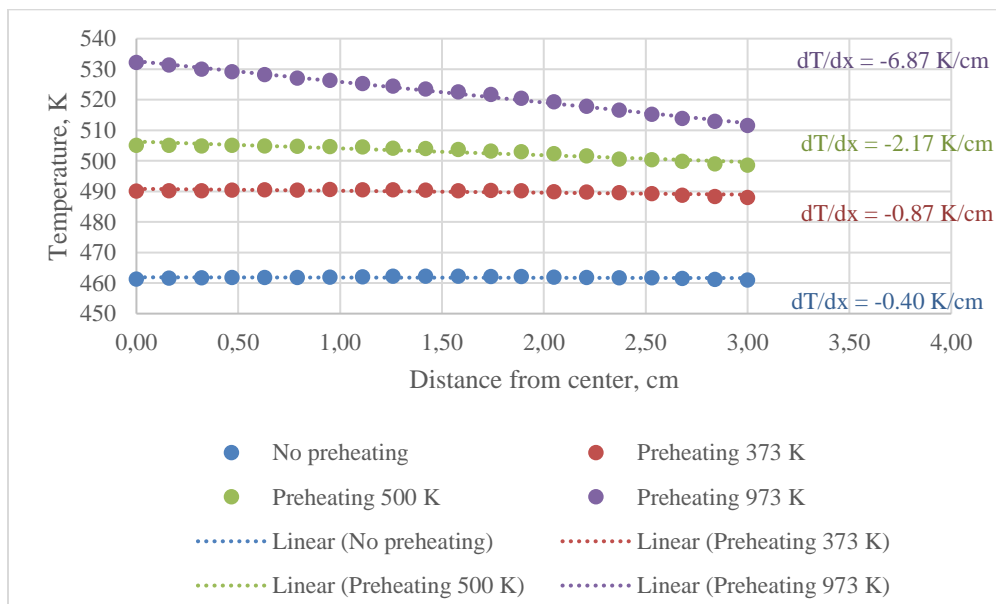


Figure 20: Reactor temperature of 500 K, residence time of 500 ms. Plots of the temperature as a function of the location of the sample. Added are their associated dT/dx values, color coordinated.

Table 7: Tabulated the respective trend lines and R^2 values for Figure 20. The case of no preheating has a low R^2 value and is due to the trend being non-linear and is visualized when plotted on its own graph. Data for this case is provided in Figure 19.

Figure	Preheating	Trend line equation	R^2
20	None	$Y=-0.0844x+461.9$	0.0557
	373 K	$Y=-0.6328x+490.7$	0.5983
	500 K	$Y=-2.2278x+506.3$	0.8953
	973 K	$Y=-6.765x+532.6$	0.9946

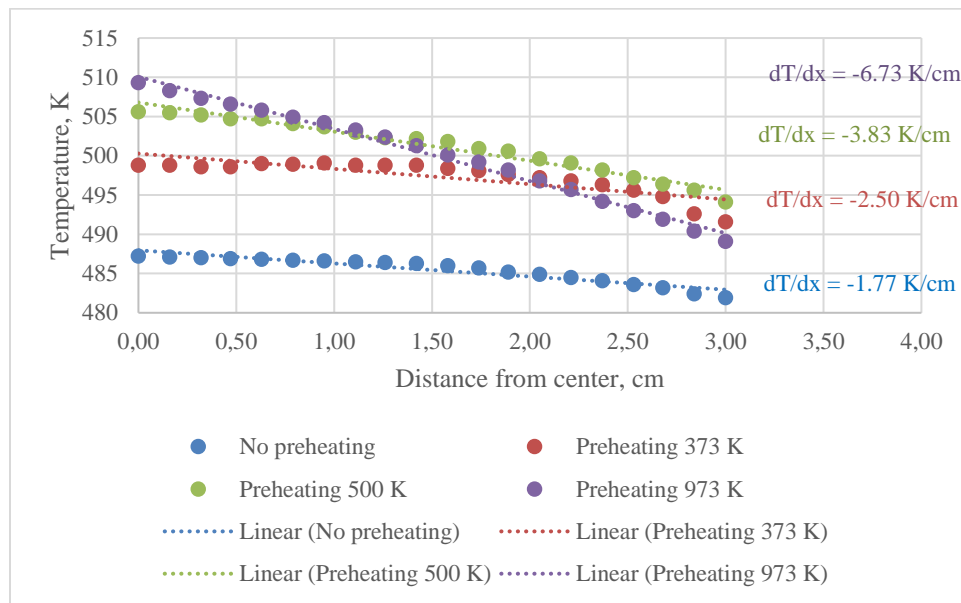


Figure 21: Reactor temperature of 500 K, residence time of 1000 ms. Plots of the temperature as a function of the location of the sample. Added are their associated dT/dx values, color coordinated.

Table 8: Tabulated the respective trend lines and R^2 values for Figure 21.

Figure	Preheating	Trend line equation	R^2
21	None	$Y=-1.6716x+488.0$	0.8971
	373 K	$Y=-1.9469x+500.3$	0.696
	500 K	$Y=-3.7077x+506.8$	0.9643
	973 K	$Y=-6.6445x+510.1$	0.9912

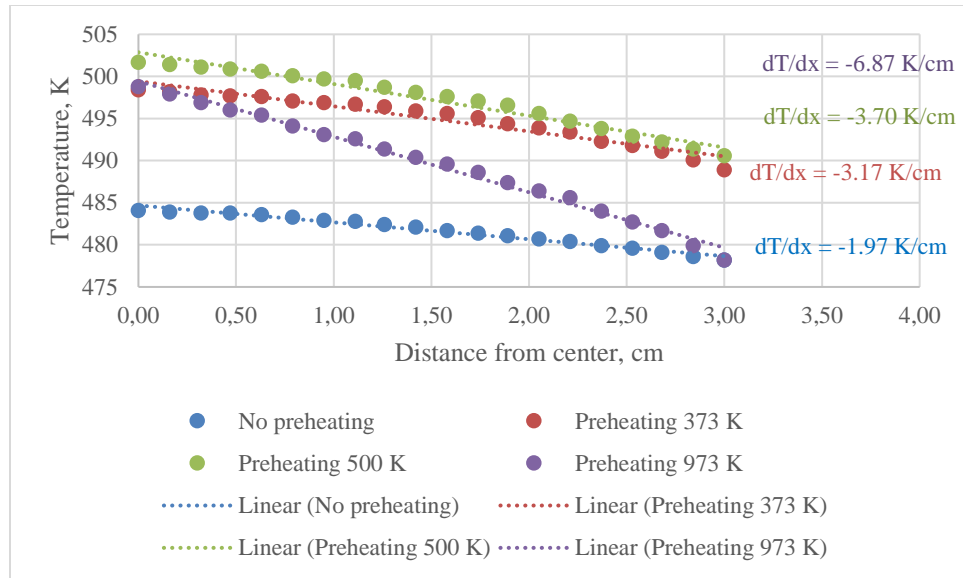


Figure 22: Reactor temperature of 500 K, residence time of 2000 ms. Plots of the temperature as a function of the location of the sample. Added are their associated dT/dx values, color coordinated.

Table 9: Tabulated the respective trend lines and R^2 values for Figure 22.

Figure	Preheating	Trend line equation	R^2
22	None	$Y = -2.008x + 484.7$	0.9777
	373 K	$Y = -2.972x + 499.4$	0.9387
	500 K	$Y = -3.7659x + 502.9$	0.9665
	973 K	$Y = -6.5868x + 499.4$	0.9919

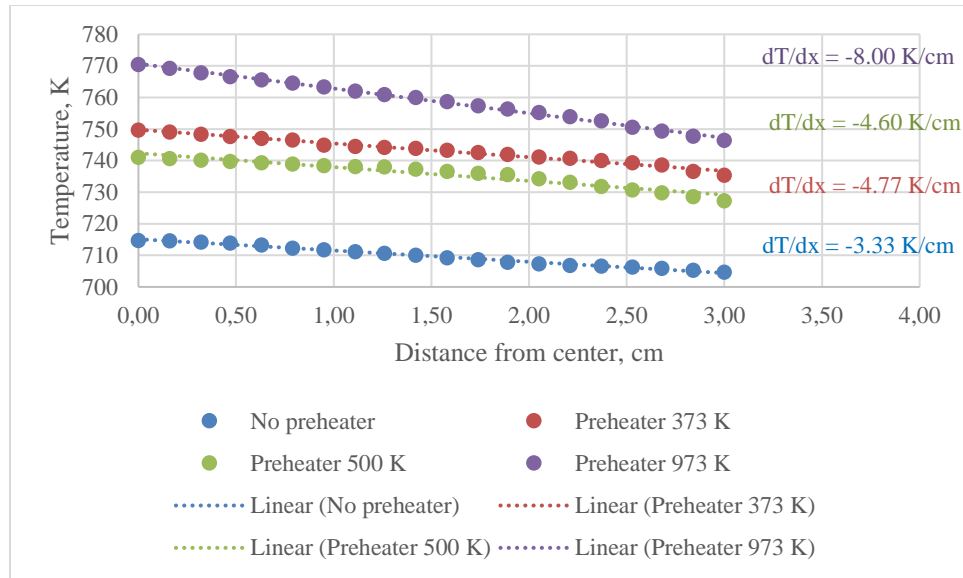


Figure 23: Reactor temperature of 750 K, residence time of 500 ms. Plots of the temperature as a function of the location of the sample. Added are their associated dT/dx values, color coordinated.

Table 10: Tabulated the respective trend lines and R^2 values for Figure 23.

Figure	Preheating	Trend line equation	R^2
23	None	$Y = -3.533x + 715.1$	0.991
	373 K	$Y = -4.3856x + 742.3$	0.9417
	500 K	$Y = -4.3393x + 749.8$	0.9841
	973 K	$Y = -7.821 + 770.7$	0.9967

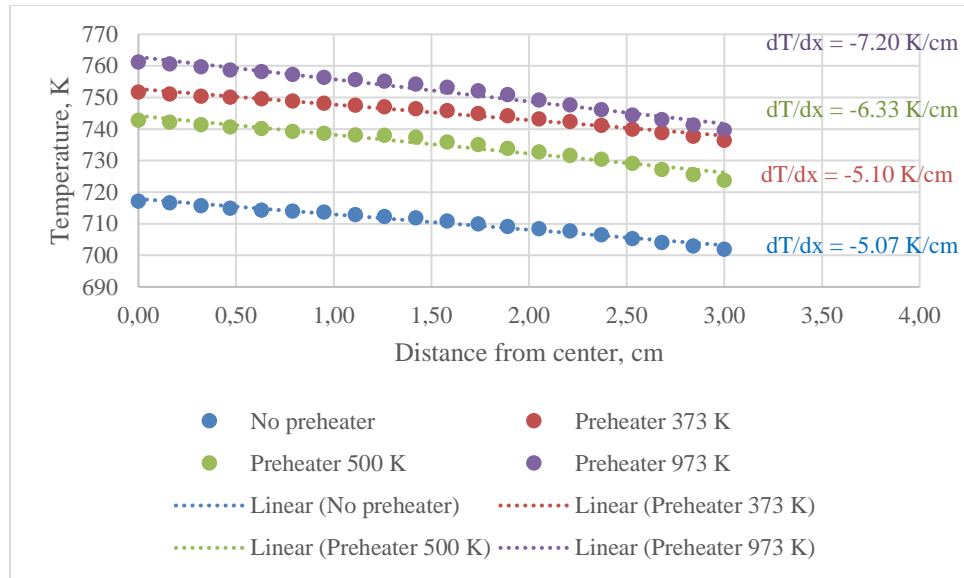


Figure 24: Reactor temperature of 750 K, residence time of 1000 ms. Plots of the temperature as a function of the location of the sample. Added are their associated dT/dx values, color coordinated.

Table 11: Tabulated the respective trend lines and R^2 values for Figure 24.

Figure	Preheating	Trend line equation	R^2
24	None	$Y = -4.8878x + 717.9$	0.979
	373 K	$Y = -4.9201x + 752.7$	0.9758
	500 K	$Y = -5.9835x + 744.2$	0.9605
	973 K	$Y = -7.0486x + 762.8$	0.9714

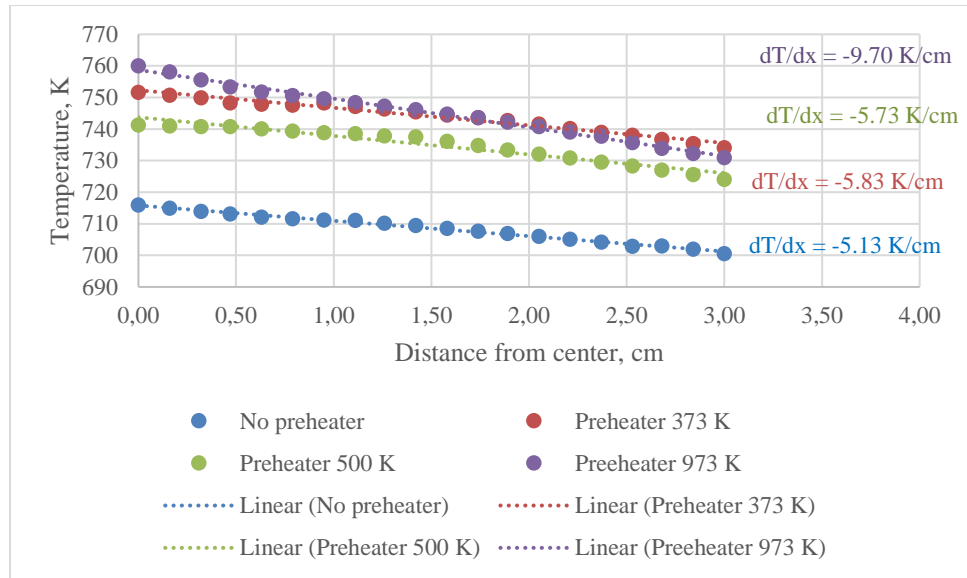


Figure 25: Reactor temperature of 750 K, residence time of 2000 ms. Plots of the temperature as a function of the location of the sample. Added are their associated dT/dx values, color coordinated.

Table 12: Tabulated the respective trend lines and R^2 values for Figure 25.

Figure	Preheating	Trend line equation	R^2
25	None	$Y = -4.8581x + 715.8$	0.9916
	373 K	$Y = -5.5642x + 752.3$	0.969
	500 K	$Y = -5.8901x + 743.7$	0.947
	973 K	$Y = -9.0934x + 758.7$	0.9931

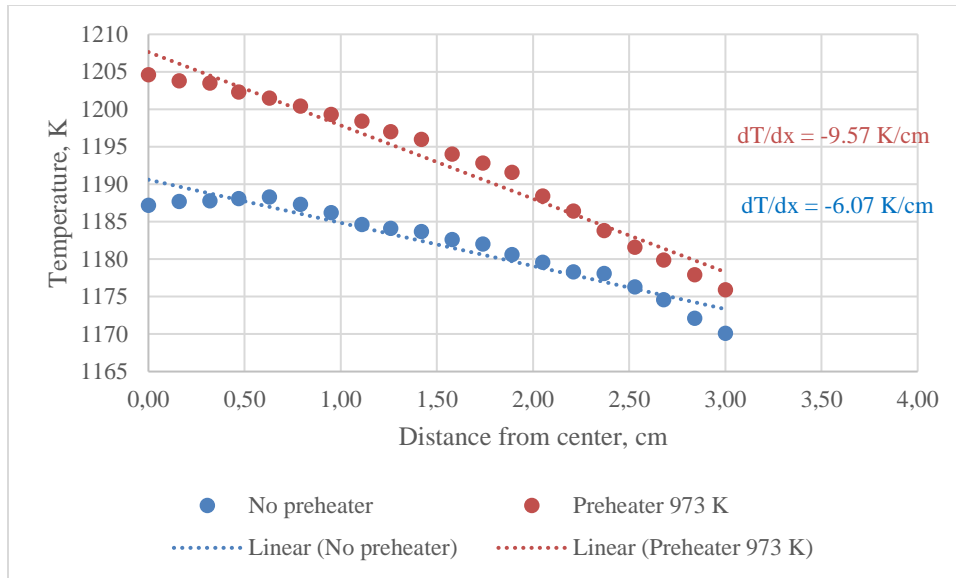


Figure 26: Reactor temperature of 1200 K, residence time of 500 ms. Plots of the temperature as a function of the location of the sample. Added are their associated dT/dx values, color coordinated.

Table 13: Tabulated the respective trend lines and R^2 values for Figure 26.

Table	Preheating	Trend line equation	R^2
26	None	$Y = -5.7577x + 1190.6$	0.9245
	973 K	$Y = -9.7892x + 1207.6$	0.9656

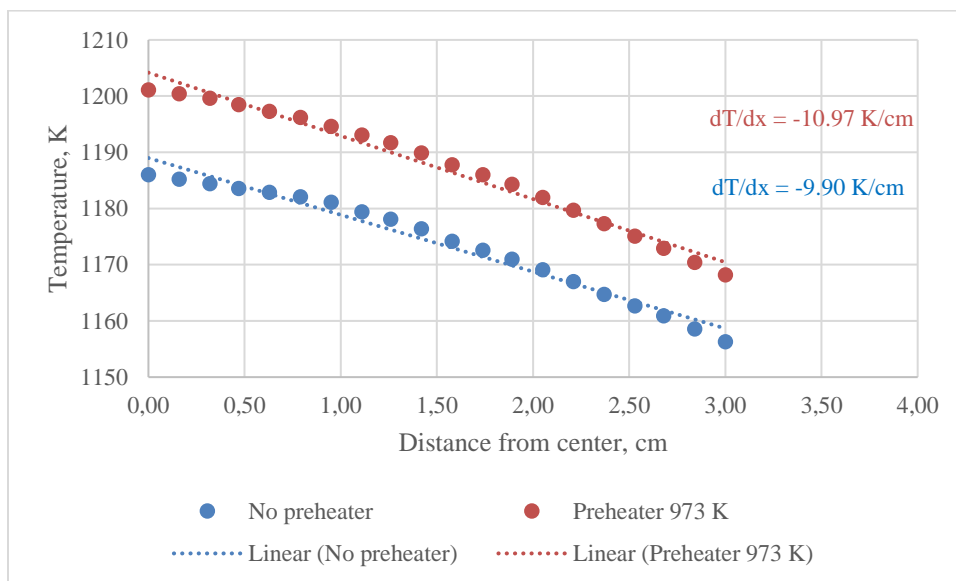


Figure 27: Reactor temperature of 1200 K, residence time of 1000 ms. Plots of the temperature as a function of the location of the sample. Added are their associated dT/dx values, color coordinated.

Table 14: Tabulated the respective trend lines and R^2 values for Figure 27.

Table	Preheating	Trend line equation	R^2
27	None	$Y = -10.109x + 1189.0$	0.9745
	973 K	$Y = -11.244x + 1204.2$	0.9807

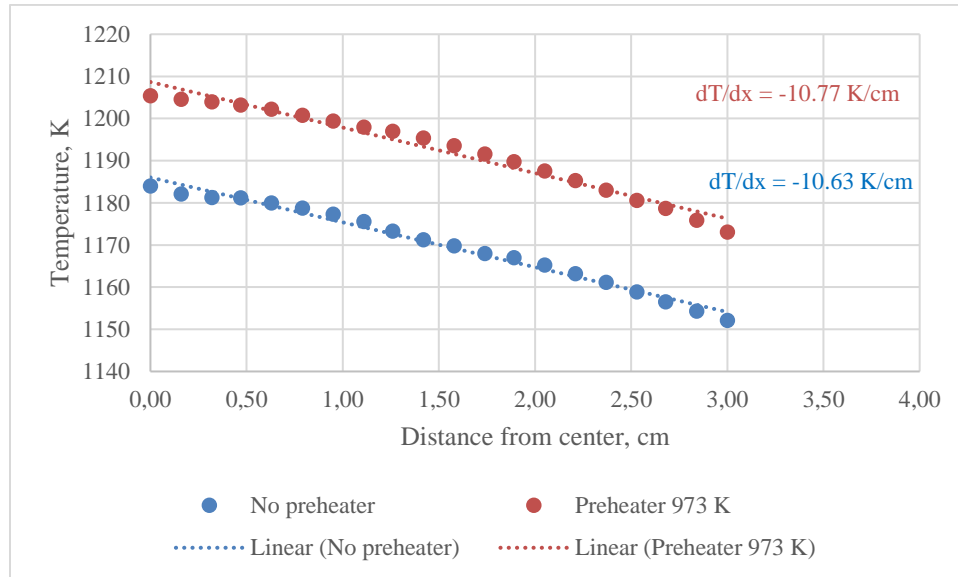


Figure 28: Reactor temperature of 1200 K, residence time of 2000 ms. Plots of the temperature as a function of the location of the sample. Added are their associated dT/dx values, color coordinated.

Table 15: Tabulated the respective trend lines and R^2 values for Figure 28.

Figure	Preheating	Trend line equation	R^2
28	None	$Y = -10.637x + 1186.0$	0.9853
	973 K	$Y = -10.804x + 1208.7$	0.9719

Based on the Figures 20-28, and their associated Tables 7-15, it is observed that the trend is very linear for most of the cases that were studied. Note that the initial temperatures do not equal each other. That is due to the fact that the experiments were not conducted under identical conditions. The experiments were conducted by using one preheating temperature, then conducting the dT/dx measurements for each residence time for a given

reactor temperature. Once completed, the next set of measurements were conducted in the same fashion, but for another preheating temperature. Table 4 was populated from left to right. This induces the different initial temperature settings for the measurements in Figures 20-28. To compare the initial temperatures, three separate figures must be analyzed, where the preheating temperature (and reactor temperature) is the same for three different flow rates. For example, the blue trend line (case of no preheating) may be comparable with the other blue lines for Figures 20-22, but not with the other cases. When that analysis is conducted, it becomes apparent that there is not a clear trend that is consistent for all reactor temperature measurements. This is due to the selection of preheating temperatures. The preheating temperatures were selected to analyze the impact of unfavorable conditions, as the ideal situation would be to have the preheating temperature equal that of the main heater to reduce the thermal gradient as the gas approaches the reaction volume. To reduce the slope of the heat decrement inside the reaction volume, it is favorable for the gases to be at the desired temperature when it reaches the jets and begins the transition from laminar flow to turbulent flow. An apparent trend that is consistent for all reactor temperature measurements is that for a given reactor temperature and preheating temperature, the case with the shortest residence time always results in the lowest dT/dx value. As the residence time decreases, the more turbulent the flow becomes, as the flow velocity is increased and yields higher rates of convective heat transfer, and, thus, a more uniform flow field.

While it is important to take the initial temperatures into consideration, what is of higher importance is the trend lines and their associated slope (dT/dx), and their regression coefficient, R^2 , which indicates how well the data fits on a linear trend line

model. In general, the R^2 increases as the residence time increases for each reactor temperature. However, more importantly, the R^2 increases as the preheating temperature increases. This is important because it emphasizes the importance of preheating the gas prior to entering the reaction volume. The fact that the temperature drop-off is very linear is encouraging because it validates the assumption that the reactor is operating at steady conditions and that the process is constant. The preexisting assumption of uniform temperature throughout the reaction volume was to be validated, and this experiment invalidates that assumption. However, it provided useful information, such as the temperature reduction is linear in relation to the location inside the reactor. That information may suggest that the outer geometry affects the temperature reading, as the reaction volume receives convective heating from 360° . Figure 29 contains an image of the reaction volume and its nozzles that connect to the cylindrical portion of the reactor. From that picture, it is clear that there is a lot of empty space between the reaction volume and the heater, as the thermocouple position travels down towards the throat. Thermal conductivity of the Inconel metal is 14.9-27.5 W/m*K for temperatures of 298-1073 K [3], as compared to that of N_2 , which is 0.030-0.087 W/m*K for temperatures of 298-1473 K at atmospheric pressure [11]. The thermal conductivity of Inconel is approximately 50,000% higher than that of N_2 , providing that the gap space could be a culprit for the temperature decrement, as the gap between the Inconel and the outer diameter of the reaction volume can be assumed negligible (only one sheet of ~ 0.1 mm thick paper could fit between the glass and Inconel). This is also the location (in 2-D) that marks the center of the reaction volume, and where the temperature was consistently the hottest in the gradient measurements.



Figure 29: Reaction volume of the JSR inside its main heaters. A clear gap is shown as the geometry changes.

The uncertainty of the K-type thermocouple itself, which standard error for K-type, is 2.2 °C or $\pm 0.75\%$ of the temperature (in units of °C), whichever is greater [12]. An investigation of the thermal gradients, dT/dx , was conducted at three different reactor temperatures: 500 K (227 °C), 750 K (477 °C), and 1200 K (927 °C). This results in thermocouple uncertainties of 2.2 °C for the 500 K case, 3.6 °C for the 750 K case, and 7.0 °C for the 1200 K case. As the temperatures in each direction did not always equal at the same position in both directions, it was of interest to investigate whether the measurements were within the thermocouple's uncertainty. To apply the uncertainties

from the thermocouple itself, a subtraction of the downstream value from the upstream value was taken, at each location, x . This resulted in a value for each location, x , and was then plotted versus each location, x , providing a detailed description of the underlying instrument uncertainties. This permitted for an analysis if the different values stems from heater uncertainties, or if the thermocouple is still accurate, or a combination of them both. Upon analysis, it was deduced that the vast majority of data points were within the uncertainty of the thermocouple, which are indicated with black lines in Figures 30-38, where each data point was allowed a ten minute period to equilibrate the thermocouple to the new environment.

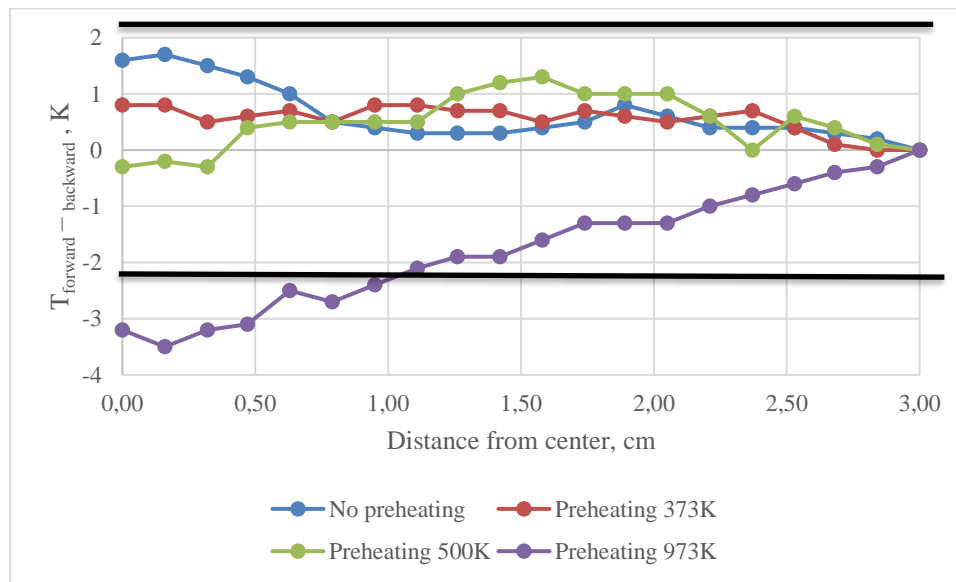


Figure 30: Reactor temperature 500 K, residence time of 500 ms. All of the data points are within the uncertainty bounds (black horizontal lines) of ± 2.2 °C, except approximately 1/3 of the measurements conducted with a preheating of 973 K.

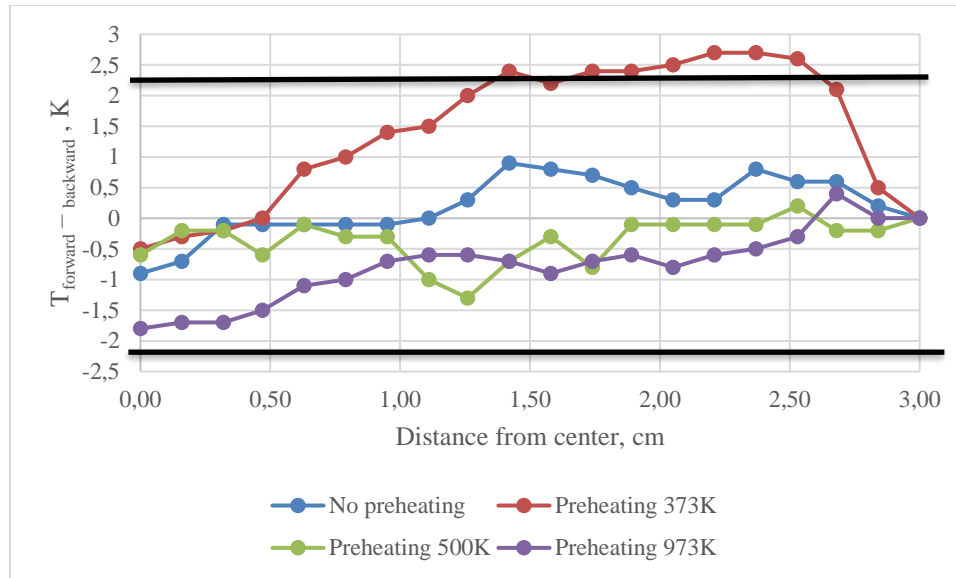


Figure 31: Reactor temperature 500 K, residence time of 1000 ms. All of the data points are within the uncertainty bounds (black horizontal lines) of ± 2.2 °C, except a few outliers for the 373 K preheating measurements.

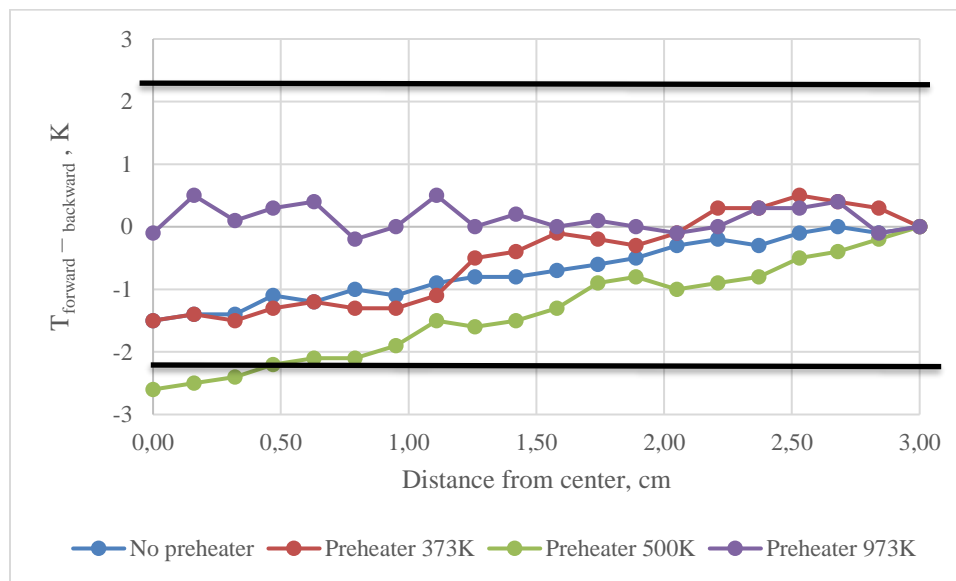


Figure 32: Reactor temperature 500 K, residence time of 2000 ms. The majority of the data points are within the uncertainty bounds (black horizontal lines) of ± 2.2 °C.

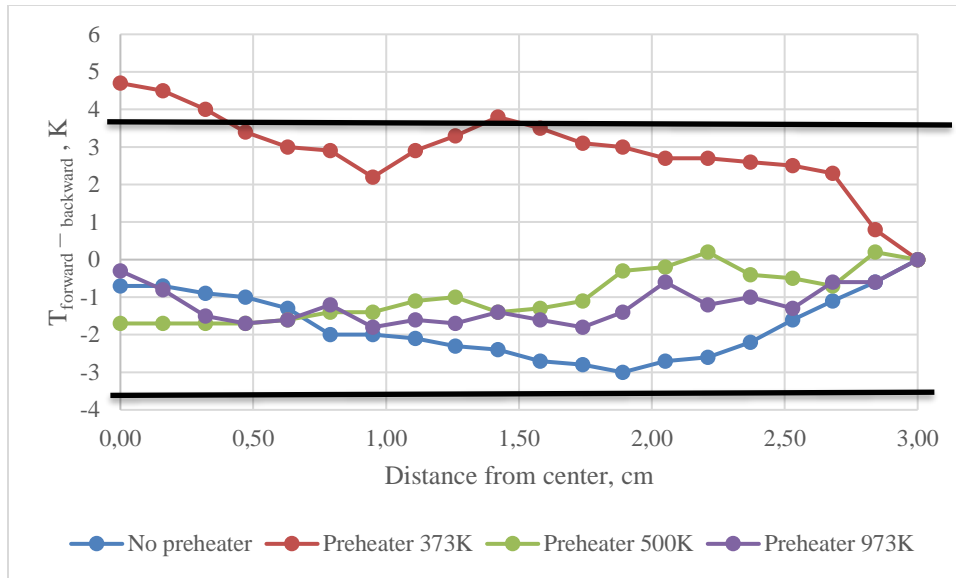


Figure 33: Reactor temperature 750 K, residence time of 500 ms. All of the data points are within the uncertainty bounds (black horizontal lines) of ± 3.6 °C, except a few outliers.

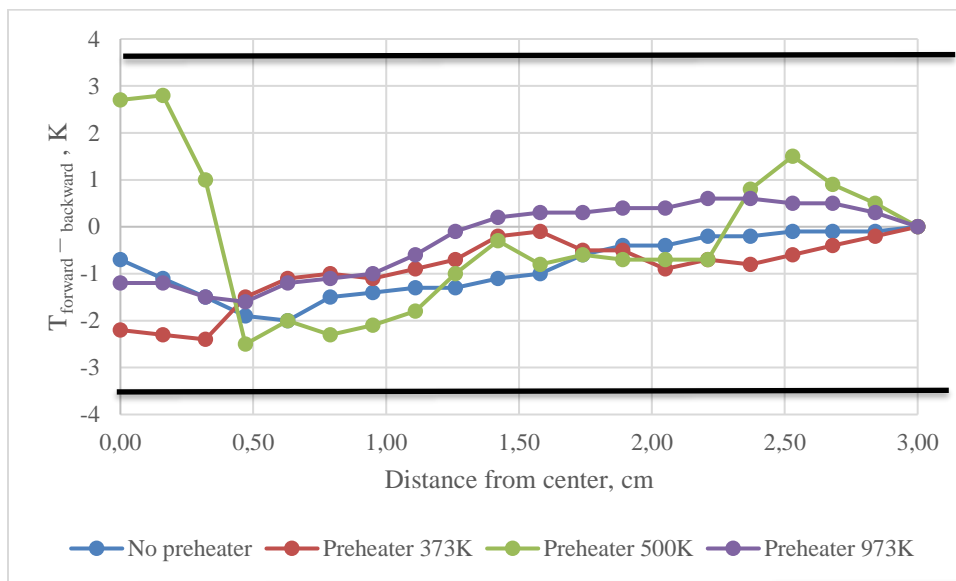


Figure 34: Reactor temperature 750 K, residence time of 1000 ms. All of the data points are within the uncertainty bounds (black horizontal lines) of ± 3.6 °C.

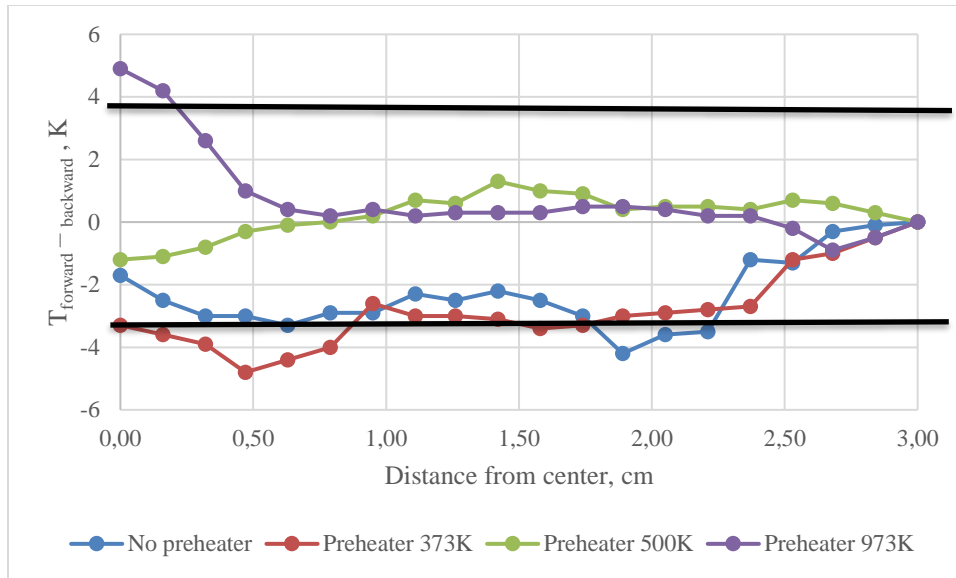


Figure 35: Reactor temperature 750 K, residence time of 2000 ms. The majority of the data points are within the uncertainty bounds (black horizontal lines) of ± 3.6 °C.

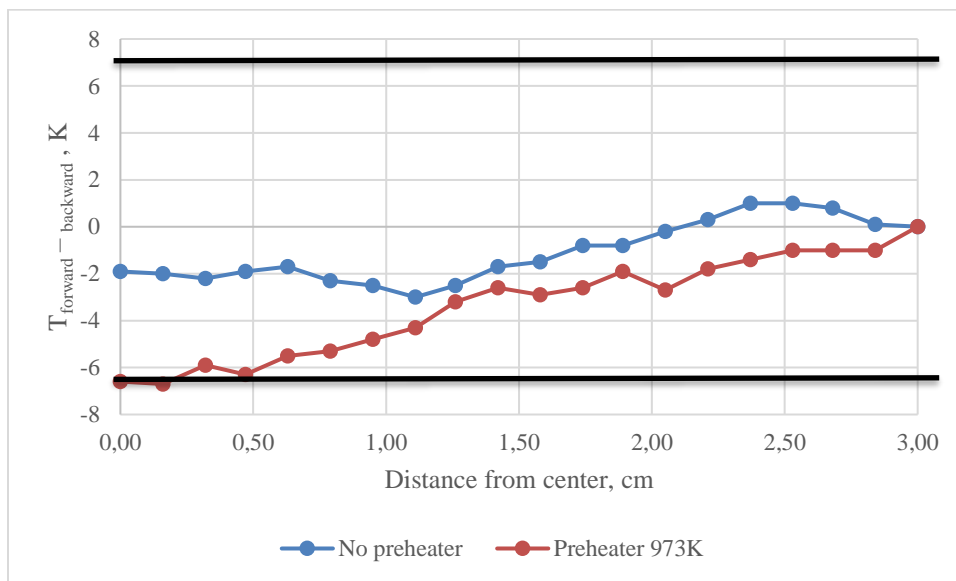


Figure 36: Reactor temperature 1200 K, residence time of 500 ms. All of the data points are within the uncertainty bounds (black horizontal lines) of ± 7.0 °C.

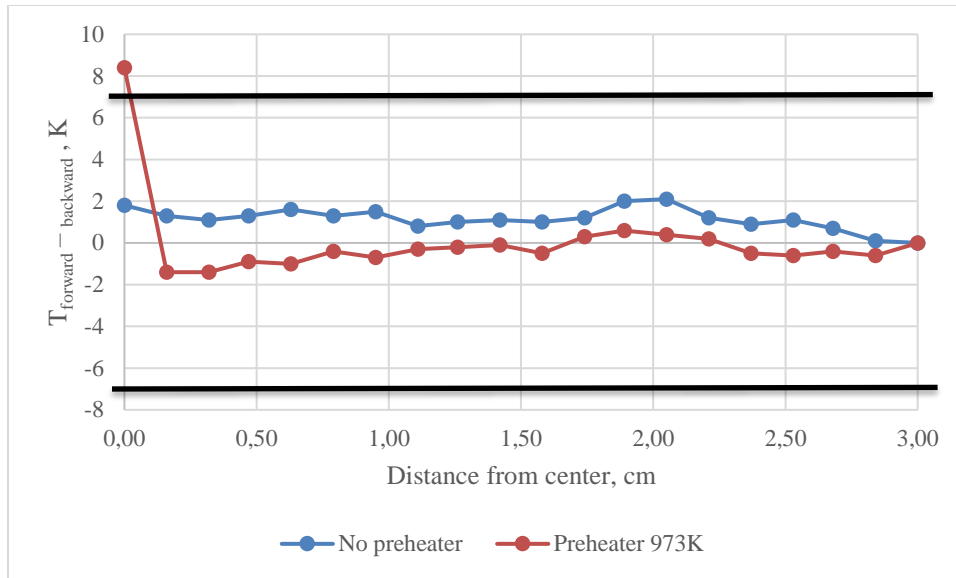


Figure 37: Reactor temperature 1200 K, residence time of 1000 ms. All except one of the data points are within the uncertainty bounds (black horizontal lines) of ± 7.0 °C.

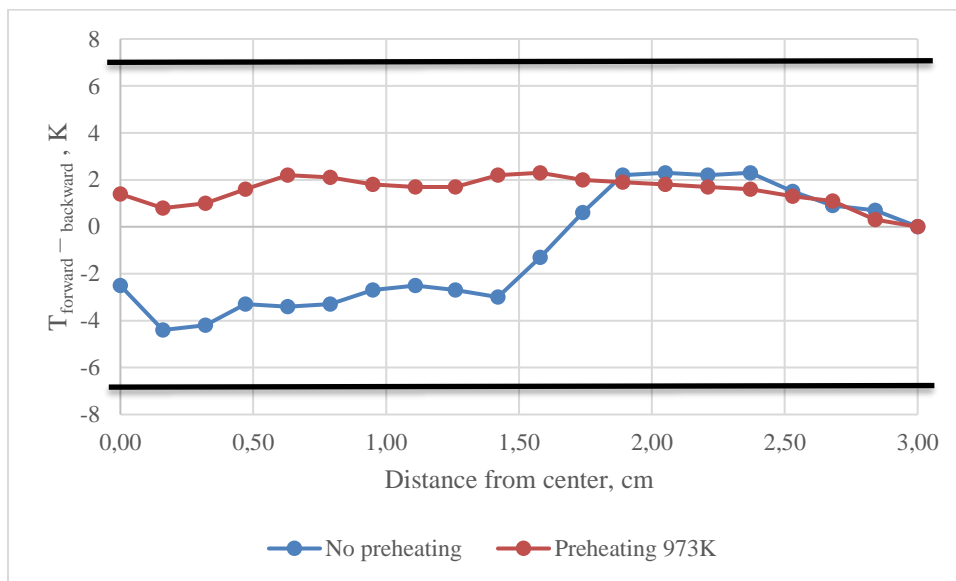


Figure 38: Reactor temperature 1200 K, residence time of 2000 ms. All of the data points are within the uncertainty bounds (black horizontal lines) of ± 7.0 °C.

Another contributing uncertainty to the temperature readings is the uncertainty from the heating source itself, which comes from the use of variable transformers (variacs), whose sensitivity is 1 V. To obtain the correct temperatures for the temperature gradient experiments, a general study on voltage-to-temperature study had to be

conducted. The goal was to find a correlation between the voltage and temperature inside the reactor, thus being able to regulate the temperature conditions with greater control. This was also studied to verify the relationship was linear, as the heating elements inside the reactor are designed to be. Six different voltages were studied: 15, 22, 30, 45, 55, and 65 V DC, respectively. Those voltages resulted in temperatures ranging from 122 °C to 870 °C, when measured using the thermocouple probe. The heaters inside the reactor are all fitted with brazed-on thermocouples: one on the top and bottom preheaters, respectively, one on the top and bottom of the main heaters, respectively, and one on the side of each main heater. This is useful because it makes it possible to track the temperatures throughout the reactor, in the event one of the heaters needs a higher or lower voltage to stabilize the temperature. The study also provides trend lines that can be used to estimate voltages for specific temperatures that are of interest to combust biofuels at. While there are in total six thermocouples embedded on the four separate heaters, only the voltages for the heaters can be adjusted, namely the top and bottom preheaters, and top and bottom main heaters, respectively. Figures 39 and 40 contain the temperatures of each heating element as a function of voltage, with accompanying trend lines added to the figure.

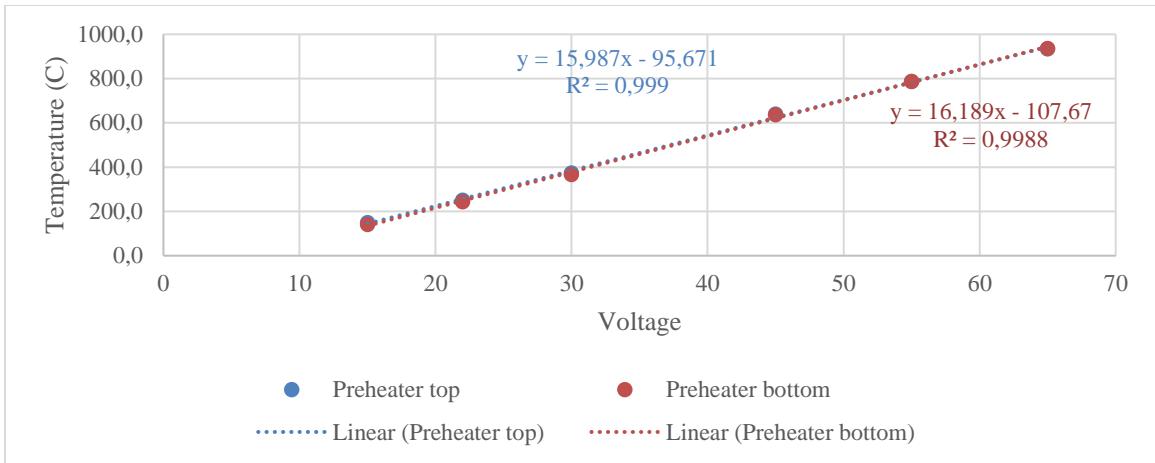


Figure 39: Preheater temperature as a function of voltage supplied by the variable transformer.

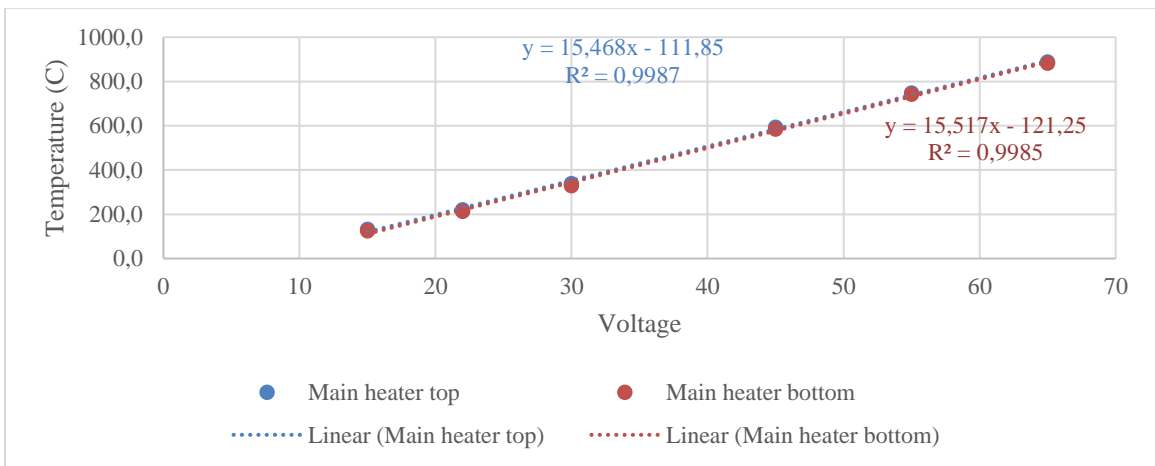


Figure 40: Main heater temperature as a function of voltage supplied by the variable transformer.

	A	B	C	D	E	F	G
1		T = f(V) equation	Set Voltage		Voltage	Temperature (°C)	Temperature (K)
2	Preheater Top	y = 15.941x - 94.799	49,9		55	782,0	1055,0
3	Preheater Bottom	y = 16.127x - 106.49	50,0		55	780,5	1053,5
4							
5	Main Heater Side Top	y = 15.144x - 105.95	53,2		55	727,0	1000,0
6	Main Heater Side Bottom	y = 15.267x - 117.98	53,6		55	721,7	994,7
7							
8	Main Heater Top	y = 15.363x - 109.85	52,7		55	735,1	1008,1
9	Main Heater Bottom	y = 15.399x - 118.99	53,2		55	728,0	1001,0
10							
11	Probe	y = 15.198x - 119.3	53,9		55	716,6	989,6
12							
13		Celsius	Kelvin				
14	Desired Temperature	700	973				

Figure 41: Calculator used to calculate voltages based on the trend lines from the inclusive study. A desired temperature is entered into cell B14, and red cells in the C column auto populate to the required set points. The blue cells in the E column may be entered manually to see what a certain voltage corresponds to in temperature.

Figure 41 contains the equations that were concluded from the trend lines in figures 39 and 40, and were integrated into an Excel spreadsheet to be used as a calculator. That was done to make the calculator more user-friendly, where the user need only enter the desired temperature and the required voltages will auto populate. A caveat that must be mentioned is that the equations were obtained and most accurate for the case when the preheating temperature setting equals that of the main heaters'. For the cases that were investigated in the aforementioned section *JSR Temperature Measurements*, the majority of the measurements required preheating temperatures differing from the main heating. This presented a slight challenge but was easily managed by adjusting either the preheating sections or main heating sections by a few volts, depending on the experimental requirements. The only downside to that solution is the time it requires to stop fluctuating and reach steady state. It is not until steady state is reached that the temperature may be assessed and adjusted accordingly. A time study was conducted to approximate the time required to make a significant temperature increase, and is presented in Figure 42. Even after approximately two hours, it is still increasing. While

the experiments of study did not commence until the temperature reading reached steady state, it is an obvious trend that on the order of a few hours are necessary.

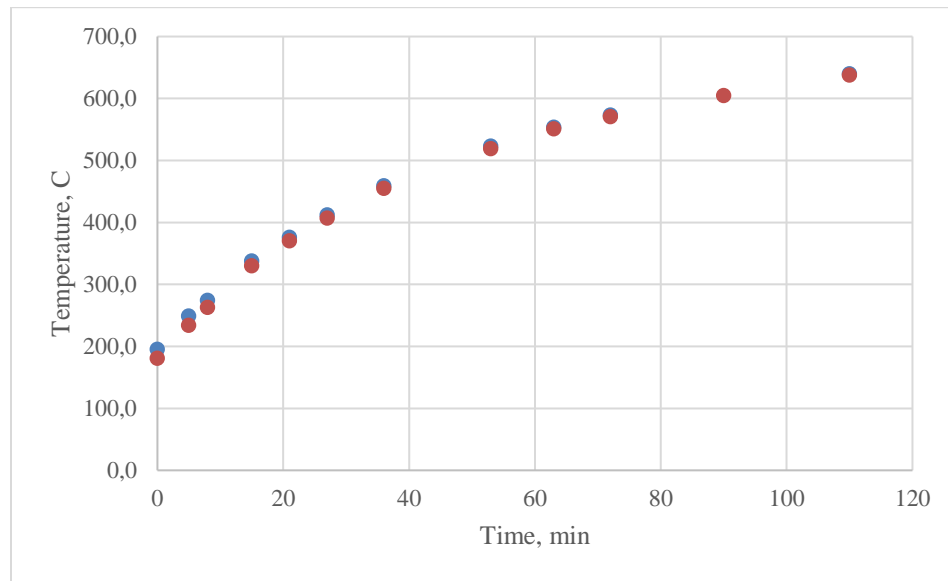


Figure 42: Time study for the side main heater thermocouple when adjusting the voltages to 55 V on the variable transformers from an initial value of 22 V.

CHAPTER 5

IMPACT OF UNCERTAINTY ON CROSS-SECTIONS AND SPECIES PROFILES

As introduced in Chapter 1, the Arrhenius equation (Equation 3b) is the backbone of gas-phase chemical kinetics, and having a fundamental understanding of the implications of inaccurate temperature readings is of utmost importance, as inaccurate temperature readings can be detrimental. There was a clear trend from the temperature gradient measurements, with the greatest dT/dx equal to 11.77 K/cm (≈ 35 K across the 3.00 cm measurement span) and occurred at the reactor temperature of 1200 K, preheating of 973 K, and a residence time of 500 ms. It is crucial to be mindful that a different temperature reading will have a significant impact on the chemical kinetics, as proven in Figure 4. Temperature is exponentially dependent in the Arrhenius equation, and if the measurement that induced a difference of 35 K from the center of the JSR to the converging-diverging nozzle is assumed to be 0 K, inherently the reaction rate, k , will be skewed. This will in turn affect ignition properties, flame propagation properties, and molecular decompositions. The reason for this investigation is to be able to account for the uncertainties within the data. As intermediates decompose into different fragmentation patterns in a direct correlation to the temperature, being able to report the jurisdiction of the data will provide clarity to what products are or could be formed, and their respective concentrations. This is why it was important to conduct an uncertainty analysis on the chemical mixture and VUV combination setup, as it is used to identify

species that are formed from combustion. If the uncertainty is too large, the graphs produced by the VUV will differ too much for the library to recognize the compound. Figure 41 illustrates how a sample VUV spectra looks when uncertainty bounds have been applied. Measurements that are analyzed in a VUV will seldom have an uncertainty greater than 5%, as chemical purity is the most attributable source. However, to visualize the effects of uncertainty, Figure 43 has an applied uncertainty bound of $\pm 5\%$ in the vertical direction.

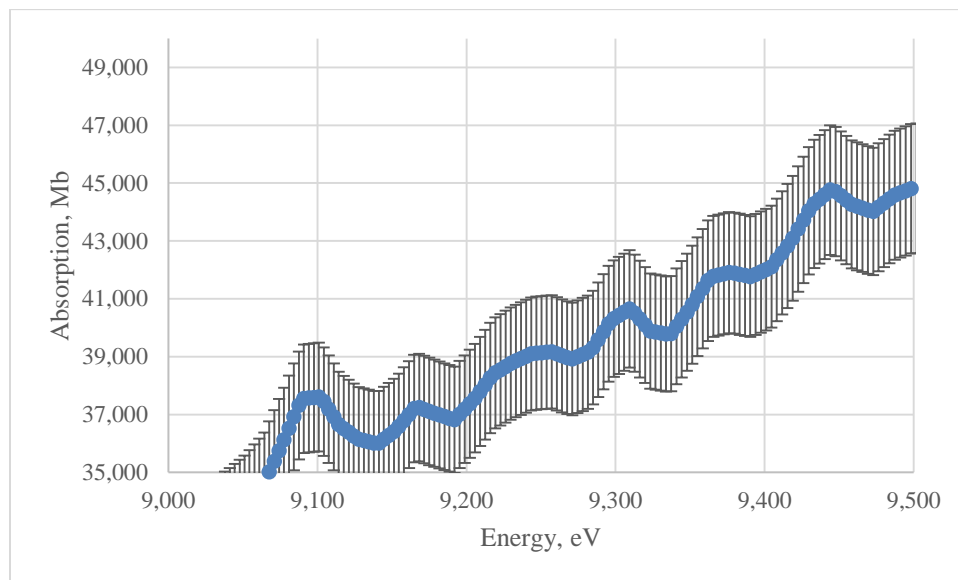


Figure 43: VUV spectra of cyclohexane. Blue line is the experimental data. Black lines are error bars of $\pm 5\%$, which is the highest uncertainty that is expected. Chemical purity is the largest source of error.

The difference is rather extreme and emphasizes the importance of accounting for the uncertainties in measurements. For combustion applications, the likelihood of an increased uncertainty increases for each instrument that is added to the equation. When a fuel is injected into the JSR, it will come with an uncertainty in overall concentration. Add the effects of temperature uncertainties and the combustion stage will incur further uncertainties. Figure 43 only accounts for the overall uncertainty when creating a chemical mixture in the manifold. Thus, it is conclusive that the global uncertainty will

increase when the effects from the JSR setup is added to the equation. Uncertainties do not necessarily mean that the data is inaccurate, but rather emphasizes the bounds to which the data is expected to fall within, which adds a confidence level. Using the uncertainty analyzes provides the opportunity to produce periodic checks to ensure the equipment is still functioning as expected and make any necessary improvements.

In summary, the following are the takeaway points from the impact of uncertainties on data that concern combustion and speciations of species:

- Mass flow controllers: A flow uncertainty methodology was developed for routine assessment of flow controller accuracy. Initial measurements were conducted.
- Cross-section uncertainty: Uncertainties were quantified in all cases by accounting for errors in gas-phase concentration. Convolving the sources of error using the root-sum-square method led to an upper limit of uncertainty above the detection limit, which is largely attributable to chemical purity.
- Time study: It takes the probe thermocouple approximately ten minutes to stabilize the temperature readout.
- Trends in dT/dx : dT/dx trends were found to increase with increasing residence time, preheating, and reactor temperature.
- Temperature difference between top and bottom preheaters and main heaters:

Figure 41 included the equations that relate variac voltages to heater temperatures.

In general, the top gets slightly hotter than the bottom for the same applied voltage. This is adjusted via increasing the bottom heaters by 1 V.

CHAPTER 6

CONCLUSIONS AND FUTURE WORK

The experiments in the present work were conducted to quantify uncertainties related to absorption cross-section measurements and JSR experiments. Thorough detailing of uncertainties are not routinely represented in other JSR facilities. Careful consideration to experimental procedures is important particularly for cases where species concentrations are ~ppm. Quantifying global uncertainty allows for the interpretation of data to be conducted with high confidence in its accuracy.

While the present work focused on thermal gradients formed inside the reaction volume of the JSR, there will be a need for future investigation to conduct an uncertainty analysis for other elements in the JSR experiment. To expand on the present work and make further improvements, a series of recommendations are in place:

- To improve the MFC uncertainty analysis, it is suggested to flow gases into the control volume while under vacuum. This will ensure the line is filled with gas and also that the MFC will have reached its steady state flow. Begin the stop watch when the needle valve downstream to the vacuum has been closed and gases fill the control volume, and the pressure should increase.
- To assess whether the geometry of the JSR due to the ~10 mm gap between the reaction volume and the heaters (cf. Figure 29) plays a role in the induced gradient, an analysis should be performed for the same reactor temperatures of 500 K, 750 K, and 1200 K, respectively, but without gas flow. If gases are not

flowing, thermal homogeneity within the reaction volume should be obtained. If a gradient is present without gases flowing, it may suggest that the gap between the reactor and heaters are the culprit.

- Conduct a computational fluid dynamics (CFD) simulation to validate that the flow rates for the requested residence times indeed are turbulent. If not, modifications to the inner geometry may be required, such as adding a nozzle starting ~6 upstream of the reaction volume and converges as it approaches the reaction volume. Incorporating more flow-tripping components blown into glass of the cylindrical portion of the JSR to maximize turbulence generation may also be necessary.
- An uncertainty analysis will need to be conducted for the experiments that include combustion. This is important because the concentrations of the fuel will be directly affected by the uncertainty of the concentration that is supplied by a syringe pump and a Vaporization Delivery Module (VDM). The present study only assesses thermal gradients, which will be the same for combustion experiments due to the level of dilution utilized (to ensure isothermal reactions), which is > 98% N₂.
- Assess whether the thermal gradient is radially symmetric within the reaction volume. This may be done using a flexible thermocouple to radially measure temperature distributions.
- Use CFD and experimental measurements to determine if the gas dynamics within the sonic probe affects the temperature of the gas samples extracted for analysis. The sampling probe uses a method called expansion cooling, which is used to

describe when the reactants are cooled from a temperature where reaction can spontaneously occur to a temperature well below that, and essentially *freezes* the sample at time of collection. As the sampling sonic probe is not heated, it is possible that it will incur a temperature decrease before it ultimately *freezes* the sample.

- Conduct an uncertainty analysis on the pressure measurements.

Uncertainty analysis on thermal distributions within the JSR is useful because as combustion chemistry is heavily dependent on temperature, it is imperative to have as much information as possible about the reaction conditions within the reaction volume, and validate any assumptions that were made. If assumptions cannot be validated, it is important to acknowledge that and make adjustments to the procedure to either eliminate them or find a correction.

References

1. Capuano, L., *Annual Energy Outlook 2019*. 2019.
2. Richard S. Figliola, D.E.B., *Theory and Design for Mechanical Measurements*. Vol. Sixth Edition. 2015: Wiley.
3. Davis, J.C., *Design of a High-Pressure Jet-Stirred Reactor*, in *College of Engineering*. 2019, University of Georgia.
4. Sellevag, S.R.G., Y.; Miller, J.A., *Kinetics of the Gas-Phase Recombination Reaction of Hydroxyl Radicals to Form Hydrogen Peroxide*. *J. Phys. Chem. A*, 2009. **113**: p. 4457-4467.
5. Marrodán, L., et al., *Effects of Bath Gas and NO_x Addition on n-Pentane Low-Temperature Oxidation in a Jet-Stirred Reactor*. *Energy & Fuels*, 2019. **33**(6): p. 5655-5663.
6. Bugler, J., et al., *An experimental and modelling study of n-pentane oxidation in two jet-stirred reactors: The importance of pressure-dependent kinetics and new reaction pathways*. *Proceedings of the Combustion Institute*, 2017. **36**(1): p. 441-448.
7. Song, Y., et al., *The sensitizing effects of NO₂ and NO on methane low temperature oxidation in a jet stirred reactor*. *Proceedings of the Combustion Institute*, 2019. **37**(1): p. 667-675.
8. Karsenty, F., et al., *Experimental and Kinetic Modeling Study of 3-Methylheptane in a Jet-Stirred Reactor*. *Energy & Fuels*, 2012. **26**(8): p. 4680-4689.

9. Serinyel, Z., et al., *An experimental and modeling study of the low- and high-temperature oxidation of cyclohexane*. Combustion and flame, 2013. **160**(11): p. 2319-2332.
10. Burke, U., et al., *Species measurements of the particulate matter reducing additive tri-propylene glycol monomethyl ether*. Proceedings of the Combustion Institute, 2019. **37**(1): p. 1257-1264.
11. Toolbox, E. *Nitrogen - Thermal Conductivity*. Available from:
https://www.engineeringtoolbox.com/nitrogen-N2-thermal-conductivity-temperature-pressure-d_2084.html.
12. Nakos, J.T., *Uncertainty Analysis of Thermocouple Measurements Used in Normal and Abnormal Thermal Environment Experiments at Sandia's Radiant Heat Facility and Lurance Canyon Burn Site*. 2004.